https://doi.org/10.5194/egusphere-2026-2639
Preprint. Discussion started: 2 June 2026

Beyond Permafrost Observation: Long-term ALT Trajectory Classification and Causal Inference Across the Circum-Arctic CALM Network

Aymane Ahajjam[1], Mary Soaper[2], Utkarsh Gupta[3], Andrew Wilcox[4], Anai Caparó Bellido[4], Sydney Weaver[2], Sheridan Parker[5], Shishay Kidanu[2], and Timothy Pasch[5]

[1]School of Electrical Engineering and Computer Science, University of North Dakota, Grand Forks, ND, USA
[2]Harold Hamm School of Geology & Geological Engineering, University of North Dakota, Grand Forks, ND, USA
[3]Department of Psychology, University of North Dakota, Grand Forks, ND, USA
[4]Department of Earth System Science & Policy, University of North Dakota, Grand Forks, ND, USA
[5]Department of Communication, University of North Dakota, Grand Forks, ND, USA

Correspondence: Aymane Ahajjam (aymane.ahajjam@und.edu)

Abstract. Active layer thickness (ALT) is a key indicator of permafrost response to environmental change. However, its long-term variation across regions can be driven by multiple geospatial factors whose relative contributions remain difficult to disentangle. In this work, we propose a framework combining two processes: long-term trajectory classification and causal inference. Accordingly, we introduce the Active Layer Dynamics Index (ALDI), categorizing ALT time series into six classes of direction and rate of change: Rapid and Gradual Thickening, Rapid and Gradual Thinning, Transitional and No Trend. ALDI relies on nonparametric trend detection, reversal identification, and bootstrap uncertainty quantification. We then conduct causal inference using site fixed-effects and first-difference estimators to examine how environmental drivers vary across ALDI classes. Applied to 129 CALM network sites (1990–2024), ALDI identifies a 3.5:1 thickening-to-thinning ratio across the pan-Arctic and substantial regional heterogeneity. In terms of causality, thermal forcing dominates at thickening sites but is absent in thinning and transitional regimes, where hydrological and disturbance processes prevail. These class-dependent relationships were not detectable in pooled analyses, underscoring the need for trajectory-aware analysis in permafrost research.

1 Introduction

Permafrost zones, which cover approximately one fifth of the Northern Hemisphere's land surface, are undergoing accelerated temperature shifts and thaw in response to rising Arctic and subarctic temperatures (Smith et al., 2022; Obu, 2021) (see Fig. 1). As this perennially frozen ground begins to thaw, it sets off a series of physical and ecological feedback loops as organic matter that was formerly frozen becomes available for microbial decomposition, releasing gases such as carbon dioxide and methane into the atmosphere and intensifying changes to the existing thermal regimes.

Beyond its role in the global carbon cycle, thawing permafrost poses an increasing threat to infrastructure and communities in high-latitude regions. As ground ice melts, the resulting loss of structural integrity can damage roads, railways, pipelines, buildings, and airstrips (Hjort et al., 2022; Streletskiy et al., 2023). Such damage can disrupt transportation networks, critical

https://doi.org/10.5194/egusphere-2026-2639
Preprint. Discussion started: 2 June 2026

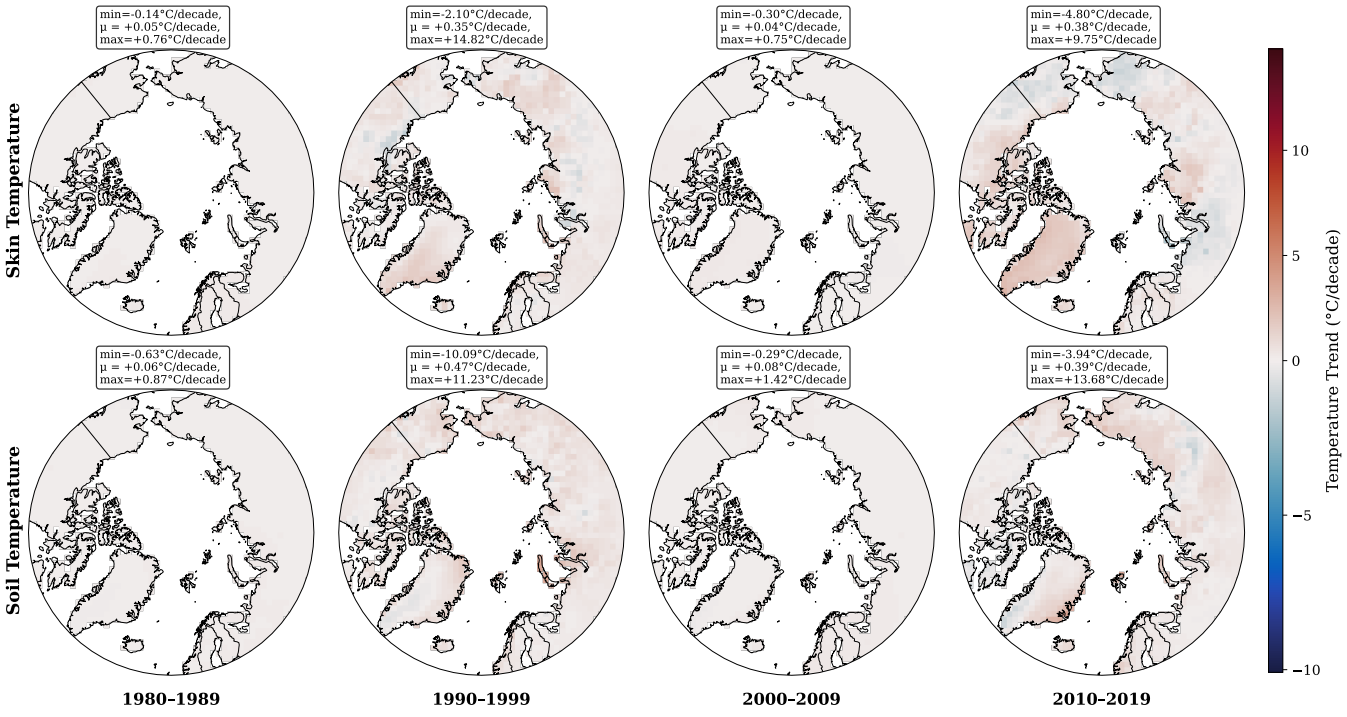

Figure 1. Decadal temperature trends across the Circum-Arctic, based on linear regression of monthly ERA5-Land data (Muñoz Sabater et al., 2021). Soil temperature represents the average across four depths ranging from 0 to 289 cm.

energy systems, and services for Arctic settlements and industrial operations. One-third to one-half of circum-arctic infrastructure may be affected by mid-century, with projected damages in the tens of billion dollars (Streletskiy et al., 2023; Hjort et al., 2022). These impacts underscore the need for spatially explicit assessments of where and how rapidly permafrost is degrading.

A key indicator of permafrost degradation is the increasing thickness of the active layer, the seasonally thawed surface layer that refreezes each winter (Muller, 1945; O'Neill et al., 2023). This metric provides a dynamic measure of thaw depth and directly reflects the balance between atmospheric forcing, surface conditions, and subsurface properties. Active layer thickness (ALT) is typically measured through mechanical probing at the end of summer, when thaw reaches its maximum depth (Brown et al., 2000). Past monitoring efforts provide valuable long-term ALT records across the circum-arctic and global permafrost region. However, sites are spatially sparse, unevenly distributed among regions, and characterized by time series that vary in length, continuity, and measurement protocols. These limitations complicate robust detection and comparison of ALT trends across the Arctic and have motivated numerous efforts to refine permafrost trend analysis.

https://doi.org/10.5194/egusphere-2026-2639
Preprint. Discussion started: 2 June 2026

2 Related Works and limitations

Understanding and predicting degradation through measurements such as ground temperature and ALT has become a main focus of permafrost research. Researchers have applied a diverse range of approaches to investigate degradation trends, including ground temperature and ALT monitoring combined with statistical time-series analysis (O'Neill et al., 2023; Biskaborn et al., 2019a), geostatistical and spatial-temporal synthesis methods (Shiklomanov et al., 2012a; Romanovsky et al., 2010), and comparative analyses of borehole and ALT records at local (Shiklomanov et al., 2010), regional (Streletskiy et al., 2015), and circumpolar scales (Brown et al., 2000). A summary of representative related works is provided in Table 1.

Extensive research conducted before and after the International Polar Year (IPY) 2007-2009 has established a trajectory of widespread permafrost degradation across the Northern Hemisphere. Global syntheses of borehole data reveal a consistent permafrost warming trend. For instance, Biskaborn et al. (2019a) quantified a global increase in permafrost temperature of roughly $0.29°C$ between 2007 and 2016, with the strongest increases occurring in the continuous permafrost zone. Regional studies corroborate this global trend, with Romanovsky et al. (2010) and Smith et al. (2010) documenting increases of roughly $0.5\text{-}2°C$ across the permafrost of Russia, with similar trends being identified in North America. In Alaska, Osterkamp (2007) highlighted that these thermal shifts in permafrost are often winter-driven, illustrating the physical consequences of rising ground temperatures.

While thermal trends are consistent, trends in the seasonally thawed active layer are more heterogeneous. The Circumpolar Active Layer Monitoring (CALM) network, established in 1991 (Nelson et al., 2021), serves as the prgesry data source for many of these assessments (Brown et al., 2000; Luo et al., 2016; Shiklomanov et al., 2012a). Analyses of ALT from CALM have produced less clear results; Luo et al. (2016) found significant ALT increases at only 43% of Northern Hemisphere sites, citing extreme spatial variability. Similarly, while Streletskiy et al. (2015) identified distinct hotspots of degradation in Western Russia, Shiklomanov et al. (2010) noted that on the North Slope of Alaska, ALT appeared statistically stable despite rising winter permafrost temperatures.

These observational discrepancies point to a key limitation in existing analyses: while ALT changes are well documented, the diversity of temporal behaviors across sites and their underlying drivers remain insufficiently characterized. Traditional trend detection approaches often rely on linear models applied to relatively short records, which can obscure differences in long-term dynamics and limit process-based interpretation.

This paper proposes a unified framework that combines long-term trajectory classification with causal inference. We introduce the Active Layer Dynamics Index (ALDI), which categorizes ALT time series into distinct classes capturing both the direction and rate of change. Building on this classification, a panel-data causal inference is conducted using site fixed-effects and first-difference estimators to identify how environmental drivers vary across index classes.

The remainder of this paper is organized as follows. Section 3 describes the study area and data used. Section 3 describes the Circum-Arctic regions as well as the CALM network employed throughout this work. Section 4 outlines the methodological framework, including the construction of ALDI and the causal inference approach. Sections 5-6 report and discusses the results and their implications in the studied regions. Finally, Section 7 concludes this paper.

https://doi.org/10.5194/egusphere-2026-2639
Preprint. Discussion started: 2 June 2026

Table 1. Summary of Related Works

Study	Data Source	Methods	Data Period	Region
O'Neill et al. (2023)	Regional Thaw Tubes (Subsidence, Thaw Pen., ALT)	Linear regression with meteorological integration; Driver analysis	1991-2018	*Northwest Canada*
Biskaborn et al. (2019a)	GTN-P borehole temperatures	Time series analysis; Linear regression & biennial mean comparisons	2007-2016	*Global Permafrost Region*
Luo et al. (2016)	CALM (ALT)	OLS linear regression (significance level: 5%)	1990-2015	*Northern Hemisphere*
Streletskiy et al. (2015)	Regional Records & CALM (Soil Temp., ALT)	Linear regression, t-test for slope significance	1963-2013	*Russian Permafrost Region*
Shiklomanov et al. (2012a)	CALM (ALT, Metadata)	Observational analysis; Spatial–temporal synthesis	1990-2010	*Circumpolar Arctic and Antarctica*
Shiklomanov et al. (2010)	CALM, CRREL, ITEX (ALT)	Geostatistical analysis; Stefan solution for ALT-TDD correlation	1960s-2009	*Utqiagvik, Alaska*
Romanovsky et al. (2010)	TSP & CALM (Ground Temp., ALT)	Comparative analysis of borehole records	1970-2009	*Russian Permafrost Region*
Smith et al. (2010)	Borehole ground-temperature observations	Observational spatial pattern analysis	1970s-2009	*Northern North America*
Osterkamp (2007)	Regional Boreholes (Ground Temp.)	Multi-site comparative analysis	1920s-2007	*Alaska*
Brown et al. (2000)	CALM (ALT)	Interannual trend analysis; Site-based comparison	1991-2000	*Circumpolar Arctic and Antarctica*
This paper (2026)	CALM (ALT); ERA5-Land; Landsat; MODIS; FIRMS	Nonparametric trend detection; Bootstrap uncertainty; DAG-informed panel causal inference	1962-2024	*Circum-Arctic region*

3 Study area and data

3.1 Circum-Arctic Region

For the purposes of this study, the circum-arctic region has been defined as the high-latitude zones (≥60°N). This expansive domain includes both continuous and discontinuous permafrost zones, shaped by complex spatial gradients in weather, vegetation, soil properties, and topography (Heginbottom et al., 1993). These environmental gradients drive considerable regional

https://doi.org/10.5194/egusphere-2026-2639
Preprint. Discussion started: 2 June 2026

variability in permafrost dynamics, with differing responses to shifts in environmental conditions observed across the Arctic (Brown et al., 2000; Heginbottom et al., 1993). As a result, the circum-arctic region serves as a critical area for assessing the spatially heterogeneous impacts of permafrost degradation amid shifting global thermal regimes.

Within this domain, permafrost conditions vary substantially across regions (see Fig. 2). In Alaska, continuous permafrost dominates the North Slope, while discontinuous and isolated permafrost are common in the interior north of 60°N, where ground ice-rich terrains are particularly vulnerable to thaw-induced subsidence. Northern Canada (including Yukon, Northwest Territories, and Nunavut) features extensive lowland tundra and peatland environments, many of which exhibit active thermokarst processes. In Greenland, permafrost is largely limited to ice-free coastal margins, most of which lie north of 60°N and are strongly influenced by maritime conditions and glacial geomorphology. Northern Fennoscandia hosts discontinuous permafrost primarily in subarctic peat plateaus and alpine zones, where it is highly susceptible to shifting surface thermal conditions. Northern Russia contains the largest expanse of continuous permafrost globally, with regions such as the Yamal

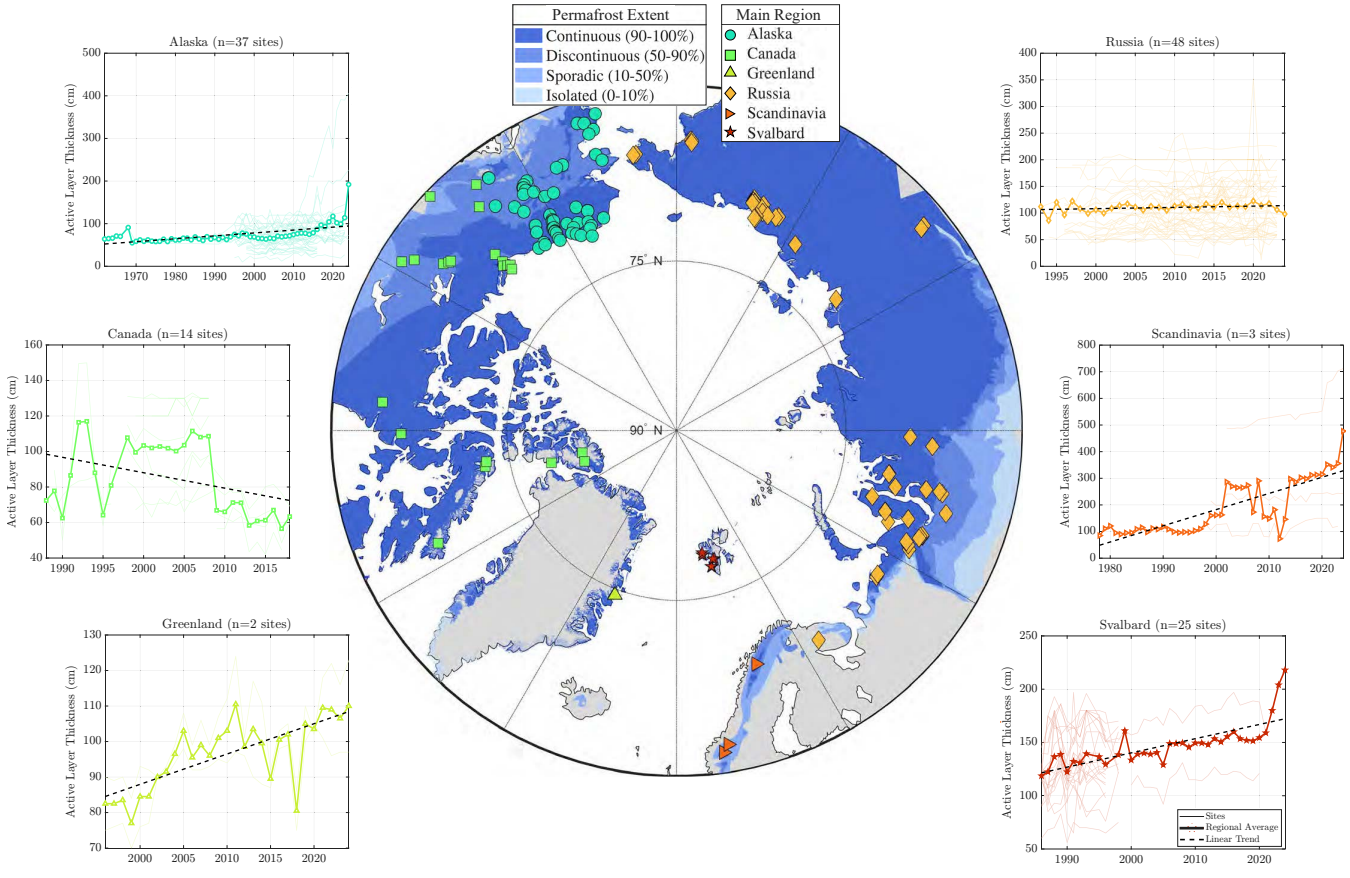

Figure 2. The circum-Arctic distribution of preprocessed CALM ALT sites overlaid on permafrost extent classes (Heginbottom et al., 2002). Time-series panels for six regions show site variability, regional averages, and long-term ALT trends.

https://doi.org/10.5194/egusphere-2026-2639
Preprint. Discussion started: 2 June 2026

Table 2. Summary statistics about the preprocessed CALM datasets. ALT values are in cm. Coverage is defined as observed years / span between first and last observation per site (in %).

Region	Sites (records)	Mean ALT	ALT range	Years range	Mean coverage
Alaska	37 (867)	77.5	[10 – 407]	[8 - 56]	94.29
Russia	48 (926)	111.9	[12 – 352.4]	[8 - 30]	94.79
Canada	14 (143)	92.1	[42 – 149.9]	[8 - 20]	95.89
Svalbard	25 (283)	134.7	[56 – 218]	[9 - 27]	88.91
Greenland	2 (58)	96.5	[70 – 124]	29	100
Scandinavia	3 (88)	230.3	[73 – 712]	[17 - 46]	90.02
Total	129 (2365)	104.8	[10 – 712]	[8 - 56]	93.99

Peninsula and Central Siberia exhibiting widespread degradation driven by high ground ice content and rapid temperature shifts.

3.2 CALM Datasets

This study uses in-situ observations from the CALM program, a long-term international initiative dedicated to monitoring ALT across permafrost regions of the Arctic and sub-Arctic (Brown et al., 2000; Nelson et al., 2021). Established in 1991, the CALM network provides standardized field measurements of seasonal thaw depth across distributed monitoring grids.

ALT measurements in the CALM network are obtained using three primary approaches: (i) thaw-tube observations based on subsurface temperature monitoring, (ii) ground temperature–based inferences derived from borehole measurements, and (iii) spatial mechanical probing conducted across regular grid or transect sampling layouts (Brown et al., 2000). In this study, observations from all three measurement types were utilized.

The original dataset gathered from the CALM platform contained 202 monitoring sites distributed across the Northern Hemisphere permafrost domain. To focus on Arctic permafrost environments, the analysis was restricted to sites located north of 60°N, resulting in 171 candidate sites. Sites are distributed across six Arctic regions including Alaska, Canada, Russia, Greenland, Scandinavia, and Svalbard. Sites were further required to contain at least eight annual ALT observations, ensuring sufficient temporal coverage for trend analysis. After preprocessing, the resulting dataset consists of 2365 annual observations from 129 sites, spanning 1962–2024. The circum-Arctic distribution of CALM monitoring sites and representative ALT time series are shown in Fig. 2, while regional statistics of the filtered dataset are summarized in Table 2.

Specifically, ALT time series vary in length across different sites and regions, ranging from 8 to 56 years, with a median of 17 years per site. The dataset contains missing data with a median coverage of 96%, defined as the ratio of observed years to the total observation span. Across all sites, ALT values range from 10 to 712 cm, with a mean of 104.8 cm and a median of 93 cm, reflecting substantial variability in active layer thickness across Arctic permafrost environments. Although the dataset

https://doi.org/10.5194/egusphere-2026-2639
Preprint. Discussion started: 2 June 2026

provides broad geographic representation, note that site locations remain influenced by logistical accessibility and proximity to research infrastructure.

4 Methods

This study proposes a two-stage analytical framework for understanding active layer dynamics across the circum-Arctic: (i) construction of the Active Layer Dynamics Index (ALDI) and (ii) causal inference of environmental drivers (see Fig. 3). Prior to analysis, the filtered CALM ALT records undergo several preprocessing steps to ensure consistency across sites and years. These include removal of non-numeric entries and conversion of censored measurements to numeric values. In addition, a negligible offset ($\sim 2 \times 10^{-4}$ °) is added to the latitude of a small number of sites to ensure unique site identifiers. Small temporal gaps ($\leq$2 consecutive missing years) are interpolated using Piecewise Cubic Hermite Interpolating Polynomials (PCHIP), which preserve monotonicity and avoid overshoot artifacts (Carlson and Fritsch, 1989). Larger gaps remain unfilled to prevent introducing artificial trends.

The first stage introduces ALDI, a categorical classification scheme that assigns each CALM site a trajectory type based on the direction, rate, and confidence of its long-term ALT trend with explicit uncertainty quantification. The second stage employs a causal inference approach grounded in permafrost physics to estimate the effects of environmental drivers on ALT, stratified by ALDI category. We note that the data and scripts used in this manuscript can be accessed via this link: https://doi.org/10.5281/zenodo.20497762 (Ahajjam, 2026).

This work was conducted on the science gateway portion of the Arctic Knowledge-Based System (A-KBS) (Wilcox et al., 2026), a Kubernetes-orchestrated environment designed to provide a platform for petascale geospatial dataset processing and intensive AI/ML workflows. The science gateway is hosted on a virtualized, load-balanced Kubernetes cluster at the University

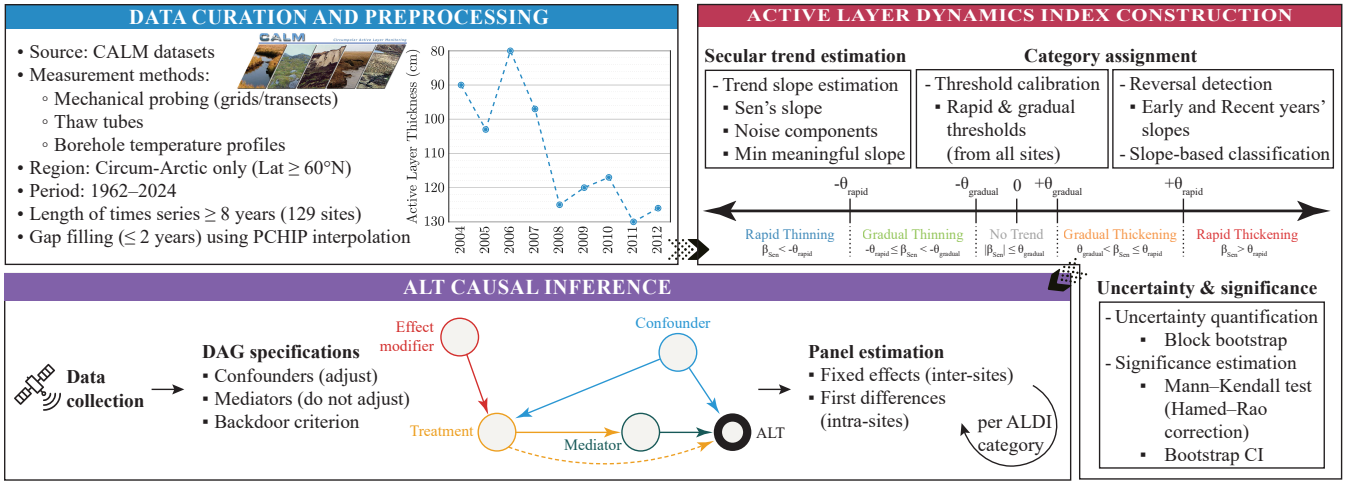

Figure 3. Conceptual diagram of the proposed framework for ALDI construction and causal inference. The first stage classifies sites into six categories with bootstrap uncertainty. The second stage estimates treatment-specific causal effects on ALT, stratified by ALDI category.

https://doi.org/10.5194/egusphere-2026-2639
Preprint. Discussion started: 2 June 2026

of North Dakota (UND) with the support of Rancher (SUSE Rancher, 2023). The gateway provides an accessible user-interface and tools for interacting with high-performance computing (HPC) resources through its integration of Globus Compute (Chard et al., 2016) and JupyterHub (Zonca and Sinkovits, 2018). In addition, the gateway's architecture enables the execution of tasks on remote resources such as the UND Talon HPC cluster and the NCSA Delta supercomputing resource, assisting researchers and decision makers working in challenging Arctic environments.

4.1 Active Layer Dynamics Index

The proposed ALDI assigns each CALM site to one of six trajectory categories that define its long-term active layer dynamics. The classification operates along two dimensions, direction and rate. Both parameters are derived from the site's estimated trend slope (see Table 3).

- Direction: captures whether the active layer is thickening (deepening over time), thinning (shallowing), showing no detectable trend, or transitional (a reversal in trend direction between early and recent periods).
- Rate: distinguishes rapid from gradual change within each direction.

Three analyses are conducted to construct the six categories: a robust trend estimator with an associated noise floor, empirically calibrated thresholds identifying the rate categories, and a reversal detection procedure for detecting transitional sites.

Table 3. ALDI classification categories. Direction is determined by the sign of β_{Sen} relative to θ_{gradual}; rate by slope magnitude relative to θ_{rapid}. Thresholds are calibrated empirically: θ_{gradual} at the 50th percentile of $|\beta_{\text{Sen}}|$ (bounded 0.10-0.30 cm yr^{-1}) and θ_{rapid} at the 80th percentile (bounded 0.50-2.0 cm yr^{-1}).

Direction	Rate	Criterion	Physical Meaning
Thickening	Rapid	$\beta_{\text{Sen}} > \theta_{\text{rapid}}$	Strong active layer deepening
	Gradual	$\theta_{\text{gradual}} < \beta_{\text{Sen}} \leq \theta_{\text{rapid}}$	Moderate active layer deepening
No trend	-	$\lvert\beta_{\text{Sen}}\rvert \leq \theta_{\text{gradual}}$	Slope below detection threshold
Thinning	Gradual	$-\theta_{\text{rapid}} \leq \beta_{\text{Sen}} < -\theta_{\text{gradual}}$	Moderate active layer shallowing
	Rapid	$\beta_{\text{Sen}} < -\theta_{\text{rapid}}$	Strong active layer shallowing
Transitional	-	$\text{sgn}(\beta_{\text{early}}) \neq \text{sgn}(\beta_{\text{recent}})$; both CIs exclude zero; both $\lvert\beta\rvert > \max(\theta_{\text{gradual}}, \beta_{\text{min}})$	Trend reversal between periods

4.1.1 Secular Trend Estimation

Trend magnitude is estimated using Sen's slope (Sen, 1968):

$$\beta_{\text{Sen}} = \text{median}\left\{\frac{\text{ALT}_j - \text{ALT}_i}{t_j - t_i}\right\} \quad \forall\, i < j \tag{1}$$

https://doi.org/10.5194/egusphere-2026-2639
Preprint. Discussion started: 2 June 2026

which is robust to outliers and requires no distributional assumptions. The value of β_{Sen} determines both the direction and rate assignment in Table 3.

To distinguish true trends from measurement noise, a site-specific minimum meaningful slope (β_{min}) is estimated from three independent noise components:

- a residual-based estimate (β_{resid}) derived from the median absolute deviation (MAD) of winsorized first differences of the detrended series,
- a quantization floor (β_{quant}) reflecting probing resolution,
- a bootstrap estimate (σ_{boot}) computed as the MAD of Sen's slope across block-bootstrap resamples.

A baseline noise level is defined as $\beta_{\mathrm{base}} = \max(\beta_{\mathrm{resid}}, \beta_{\mathrm{quant}})$. The bootstrap estimate is incorporated through a guarded maximum that discards it when it exceeds a plausible range:

$$\tilde{\sigma} = \begin{cases} \sigma_{\mathrm{boot}} & \text{if } \sigma_{\mathrm{boot}} \leq \kappa \cdot \beta_{\mathrm{base}} \\ \beta_{\mathrm{base}} & \text{otherwise} \end{cases} \tag{2}$$

$$\beta_{\mathrm{min}} = \min(\max(\beta_{\mathrm{base}}, \tilde{\sigma}),\ \beta_{\mathrm{cap}}) \tag{3}$$

where $\kappa = 4$ limits the influence of inflated bootstrap estimates and $\beta_{\mathrm{cap}} = 5.0\ \mathrm{cm\,yr^{-1}}$ prevents pathological inflation under extremely short or noisy records (Streletskiy et al., 2017).

4.1.2 Category Assignment

ALDI classification of a certain site proceeds in two steps. First, potential reversals are identified by partitioning the ALT time series into early and recent windows comprising the first and last seven calendar years for records ≥14 years, with proportionally scaled windows for shorter records (minimum 5 years per window with no overlap). Sen's slope is computed separately for each window (β_{early}, β_{recent}), and bootstrap confidence intervals are obtained for both. A site is classified as transitional when: (i) $\mathrm{sgn}(\beta_{\mathrm{early}}) \neq \mathrm{sgn}(\beta_{\mathrm{recent}})$; (ii) both bootstrap CIs exclude zero; and (iii) both $|\beta_{\mathrm{early}}|$ and $|\beta_{\mathrm{recent}}|$ exceed $\max(\theta_{\mathrm{gradual}}, \beta_{\mathrm{min}})$, ensuring the change is not merely a transition between noise and a weak trend.

Second, the remaining sites are assigned to one of the five slope-based categories using specific thresholds. Rather than imposing fixed boundaries a priori, thresholds are derived from the observed slope distribution across all qualifying sites:

$$\theta_{\mathrm{gradual}} = \mathrm{clip}\left(P_{50}(|\beta_{\mathrm{Sen}}|),\ 0.10,\ 0.30\right) \quad \mathrm{cm\ yr^{-1}} \tag{4}$$

$$\theta_{\mathrm{rapid}} = \mathrm{clip}\left(P_{80}(|\beta_{\mathrm{Sen}}|),\ 0.50,\ 2.0\right) \quad \mathrm{cm\ yr^{-1}} \tag{5}$$

https://doi.org/10.5194/egusphere-2026-2639
Preprint. Discussion started: 2 June 2026

where P_k denotes the kth percentile and bounds reflect CALM measurement precision ($\sim$1-2 cm for mechanical probing) accumulated over typical record lengths (Brown et al., 2000; Streletskiy et al., 2017). The rapid threshold is additionally constrained to be at least twice the gradual threshold to ensure category separation.

4.1.3 Uncertainty & Significance quantification

Classification uncertainty is quantified using Block bootstrap resampling (Künsch, 1989) with $B = 1000$ iterations while preserving temporal autocorrelation. Block size is set adaptively as $b = \max(2, \min(5, n/4))$, and in each iteration $\lceil n/b \rceil$ blocks are sampled with replacement, concatenated chronologically, and truncated to the original length. The bootstrap distribution yields empirical classification probabilities:

$$P(c) = \frac{1}{B} \sum_{b=1}^{B} \mathbf{1}\left(\beta_{\mathrm{Sen}}^{(b)} \in \mathcal{R}_c\right) \tag{6}$$

where $\beta_{\mathrm{Sen}}^{(b)}$ is Sen's slope from the bth bootstrap sample and $\mathcal{R}_c$ denotes the slope range defining category c. Probabilities are computed across the five slope-based categories; transitional states are identified deterministically and are not assigned probabilistic weights.

Trend statistical significance are assessed using the Mann-Kendall test (Mann, 1945; Kendall, 1975), with the variance of the test statistic adjusted via the Hamed-Rao correction (Hamed and Rao, 1998) to account for autocorrelation. Significance is assessed at $\alpha = 0.10$ to reduce Type II error (Mudelsee, 2019). A trend is considered statistically significant if either the Mann-Kendall test yields $p < \alpha$ or the bootstrap confidence interval for β_{Sen} excludes zero, and meaningful if $|\beta_{\mathrm{Sen}}| \geq \beta_{\min}$.

Statistical significance functions as a confidence indicator rather than a classification gate, aligning with permafrost literature conventions where trends are reported regardless of formal significance at individual sites (Biskaborn et al., 2019a). Confidence levels integrate both statistical significance and the signal-to-noise ratio:

- High confidence: requires both statistical significance and a magnitude exceeding the noise floor ($|\beta_{\mathrm{Sen}}| \geq \beta_{\min}$),
- Moderate confidence: requires either criterion,
- Low confidence: indicates neither is met.

We note that sites with fewer than 10 observations or a record span shorter than 12 years are additionally flagged as low statistical power.

4.2 ALT Causal Inference

To investigate whether ALDI categories capture genuine heterogeneity in environmental conditions, we estimate the causal effects of different drivers on ALT using a DAG-informed panel data approach. The analysis proceeds in three stages: causal structure specification, panel estimation, and stratification by index category.

https://doi.org/10.5194/egusphere-2026-2639
Preprint. Discussion started: 2 June 2026

4.2.1 DAG Specification and Identification

Multiple factors can impact change in ALT, including air temperature, land cover, and soil properties (Peng et al., 2018). Causal identification relies on directed acyclic graphs (DAGs) encoding the physical relationships governing active layer dynamics. The DAG structure is grounded in the Stefan equation (Zhang, 2005), the n-factor framework (Klene et al., 2001), snow insulation dynamics (Zhang et al., 1996; Ling and Zhang, 2003), and organic layer thermal effects. Eleven treatment variables were considered in this work (see Table 4).

For each treatment variable, the DAG specifies three sets of variables:

- *Confounders*: variables that causally affect both the treatment and ALT, which must be adjusted for to satisfy the back-door criterion (Pearl, 1993). These are predominantly geographic and terrain factors (latitude, elevation, continentality, slope, aspect, topographic position index) that influence both environmental drivers and active layer response.
- *Mediators*: variables on the causal pathway from treatment to ALT, which must *not* be adjusted for to avoid blocking the effect of interest. For instance, soil temperature mediates the effect of thawing degree-days on ALT via the Stefan equation; controlling for soil temperature would attenuate the estimated effect of TDD.
- *Effect modifiers*: pre-treatment characteristics (permafrost type, ground ice content, soil organic carbon) that may modify the treatment effect magnitude, used for heterogeneity analysis.

For each treatment, the minimal sufficient adjustment set is derived from the backdoor criterion applied to the treatment-specific DAG. Site fixed effects in the panel models additionally absorb all time-invariant confounders (including terrain, soil

Table 4. Treatment variables used in ALT causal inference.

Category	Variable	Description	Data source
Thermal forcing	TDD	Thawing degree days (May-Sep sum of $T_{air} > 0°C$)	ERA5-Land
	FDD	Freezing degree days (annual sum of $\|T_{air} < 0°C\|$)	ERA5-Land
	HWD	Heat-wave days (JJA days with $T_{max} > 20°C$)	ERA5-Land
Snow dynamics	SWE_{max}	Maximum seasonal snow water equivalent	ERA5-Land
	SDO	Snow-off day of year (first day in Mar-Jun with snow depth < 2 mm)	ERA5-Land
Hydrology	P_{summer}	Total summer (JJA) precipitation	ERA5-Land
	SM	Annual mean surface volumetric soil moisture	ERA5-Land
	NDWI	Summer mean Gao (Gao, 1996) NDWI (vegetation moisture)	Landsat SR
Vegetation	$NDVI_{summer}$	Mean summer (JJA) vegetation index	MODIS (2000+) / AVHRR (pre-2000)
Disturbance	FireDays	Number of wildfire detection days	NASA FIRMS
	ROS	Rain-on-snow days (Nov-Apr; snow > 5 mm, precip > 1 mm, $T > 0°C$)	ERA5-Land

https://doi.org/10.5194/egusphere-2026-2639
Preprint. Discussion started: 2 June 2026

properties, and permafrost type), providing a second layer of confounding control beyond the DAG-specified set. Table B2 details the considered 11 treatments, the adjustment sets, excluded mediators, and physical justification for each treatment.

4.2.2 Panel Estimation

Causal effects are estimated using two complementary panel data estimators applied to the site×year panel:

- Fixed effects (FE): estimates effects from within-site variation over time. Specifically, this estimator absorbs all time-invariant site characteristics through site-specific intercepts. Let ALT_{it} denote the maximum ALT at site i in year t, and would be defined as:

$$\mathrm{ALT}_{it} = \beta T_{it} + \boldsymbol{\gamma}' \mathbf{X}_{it} + \alpha_i + \varepsilon_{it} \tag{7}$$

  where T_{it} is the treatment variable for site i in year t, $\mathbf{X}_{it}$ is the vector of time-varying confounders from the DAG-specified adjustment set, with associated coefficients $\boldsymbol{\gamma}$. The parameter β captures the within-site effect of the treatment on ALT. While α_i is the site fixed effect, and ε_{it} is the idiosyncratic error term. Inference uses cluster-robust standard errors (Cameron and Miller, 2015) clustered at the site level to account for within-site serial correlation.

- First differences (FD): estimates effects from year-to-year changes within sites, removing site-specific intercepts through differencing:

$$\Delta\mathrm{ALT}_{it} = \beta \Delta T_{it} + \boldsymbol{\gamma}' \Delta\mathbf{X}_{it} + \Delta\varepsilon_{it} \tag{8}$$

  where Δ denotes the first-difference operator ($\Delta y_{it} = y_{it} - y_{i,t-1}$). The FD estimator is more sensitive to short-term variability, while the FE estimator captures the full within-site relationship. Consistency of the causal effect estimate across both estimators strengthens the causal interpretation (Angrist and Pischke, 2009).

Year fixed effects are deliberately excluded. Because meteorological treatments (e.g., TDD, precipitation) vary primarily across years, year fixed effects would absorb the temporal variation that constitutes the treatment signal, rendering the effects unidentifiable.

To facilitate cross-treatment comparison, the estimated effects are standardized, expressing ALT response (cm) per one standard deviation (SD) increase in each treatment:

$$\hat{\beta}_{std} = \hat{\beta} \times \sigma_X \tag{9}$$

where σ_X is the within-site SD for FE and the SD of first differences for FD.

To investigate whether ALT dynamics moderate environmental sensitivity, the panel estimation is repeated separately for subsets of sites belonging to individual ALDI classes. This stratified approach allows treatment effect magnitudes to differ across trajectory types. For instance, a 1 °C increase in TDD may produce a larger ALT response at Rapidly Thickening sites than at sites with no trend, reflecting differences in ground thermal properties, ice content, or proximity to thresholds. The statistical significance for causal estimates is assessed at $\alpha = 0.05$.

https://doi.org/10.5194/egusphere-2026-2639
Preprint. Discussion started: 2 June 2026

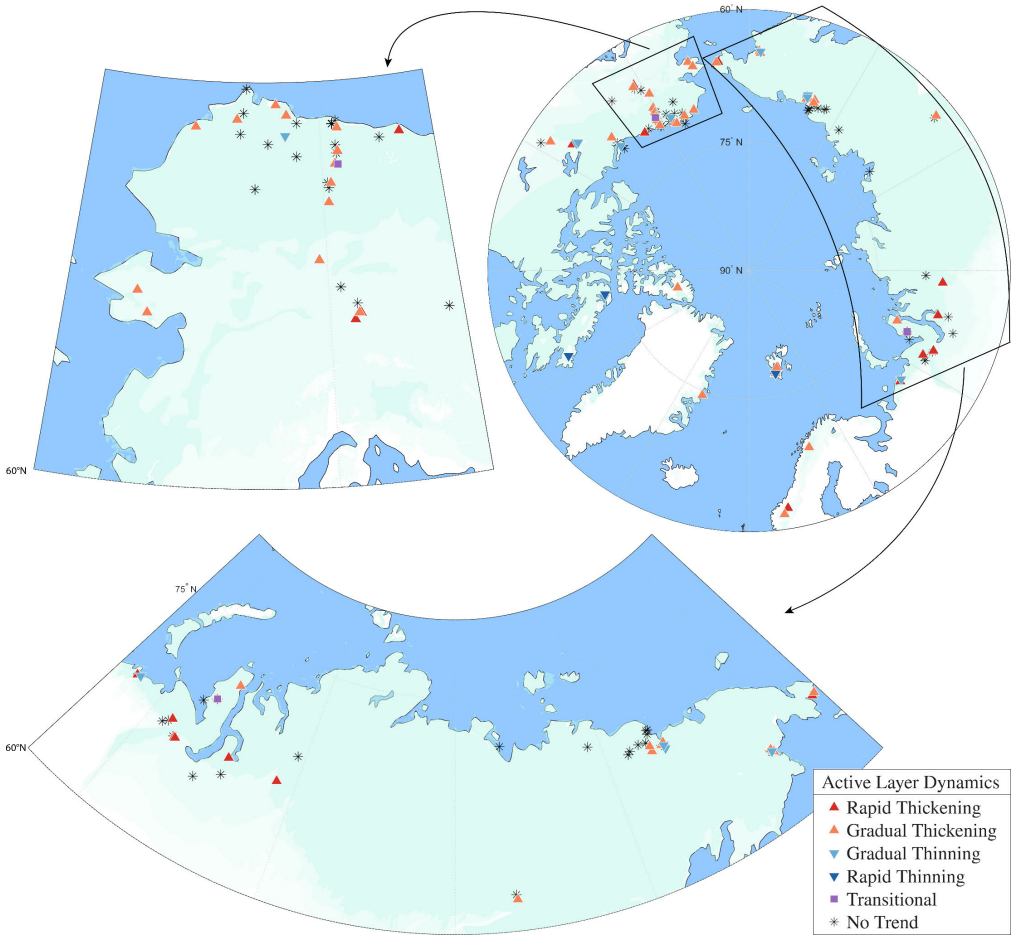

Figure 4. Spatial distribution of ALDI classes across all considered sites. Thickening classes are more widespread than thinning ones, while transitional classes are comparatively limited.

We note that of the 129 CALM sites classified by ALDI, 97 are retained for causal analysis. This is the result of excluding sites where ERA5-Land data didn't exist, which might be due to classifying the nearest grid cell as ocean due to its land-sea mask, a known limitation at Arctic coastal latitudes.

5 Results

The results are organized in two parts. The first presents the output of the ALDI classification on the ALT time series, including the Circum-Arctic wide and regional distribution of index classes, the statistical reliability of the classifications, and representative time series. The second reports the panel-data causal inference analysis, identifying the environmental drivers of active layer thickness change and examining how their effects vary across ALDI categories.

https://doi.org/10.5194/egusphere-2026-2639
Preprint. Discussion started: 2 June 2026

5.1 ALDI classification

From the 129 qualifying CALM sites, 39.5% were classified as No Trend, 27.9% as Gradual Thickening, 17.8% as Rapid Thickening, and 10.9% as Gradual Thinning, while only 3 sites were identified as Rapid Thinning and 2 as Transitional (see Fig. 4). Aggregating the directional categories, 59 sites (45.7%) exhibit thickening trajectories compared with 17 sites (13.2%) showing thinning, yielding a network-wide thickening-to-thinning ratio of approximately 3.5:1. The Mann-Kendall test identifies significant monotonic trends at 40 sites (31.0%), with higher detection rates among thickening sites (50.8%) than thinning sites (35.3%). Confidence levels reflect this asymmetry: 40 of the 51 No Trend sites have $|\beta_{\text{Sen}}|$ below their site-specific $\beta_{\min}$, indicating that these series remain within the site-level noise floor, whereas 63 of the 78 directional sites exceed their $\beta_{\min}$. Across all sites, $\beta_{\min}$ has a median of 0.31 cm yr^{-1} (IQR: 0.13-0.86) and decreases with record length (Spearman $\rho = -0.65$, $p < 0.001$), indicating that longer records resolve progressively smaller trends. Per-site results are reported in Table A1.

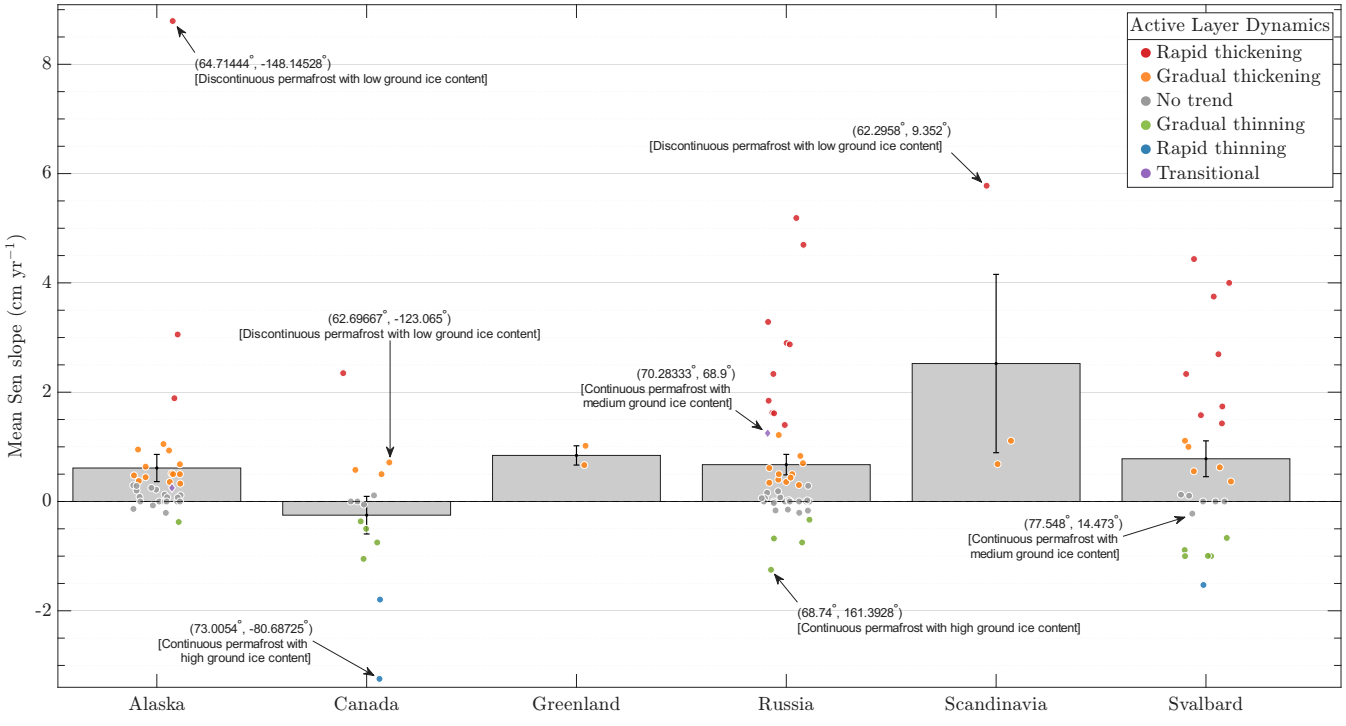

Figure 5. Regional comparison of Sen's slope estimates of ALT time series across all considered sites. Bars represent the regional mean Sen slope, with individual site-level slopes overlaid and colored by ALDI classification. Selected sites are annotated to illustrate contrasting behaviors across permafrost regimes. Permafrost zone and ground-ice content are derived from (Heginbottom et al., 2002).

These network-level proportions are also reflected in the mapped spatial distribution of ALDI classes in Fig. 4, which reveals substantial heterogeneity across the circum-Arctic CALM network. Alaska and Russia sites showcase the dominance of Thickening over Thinning classes. Along Alaska's North Slope, the related sites are largely composed of No Trend, Gradual

https://doi.org/10.5194/egusphere-2026-2639
Preprint. Discussion started: 2 June 2026

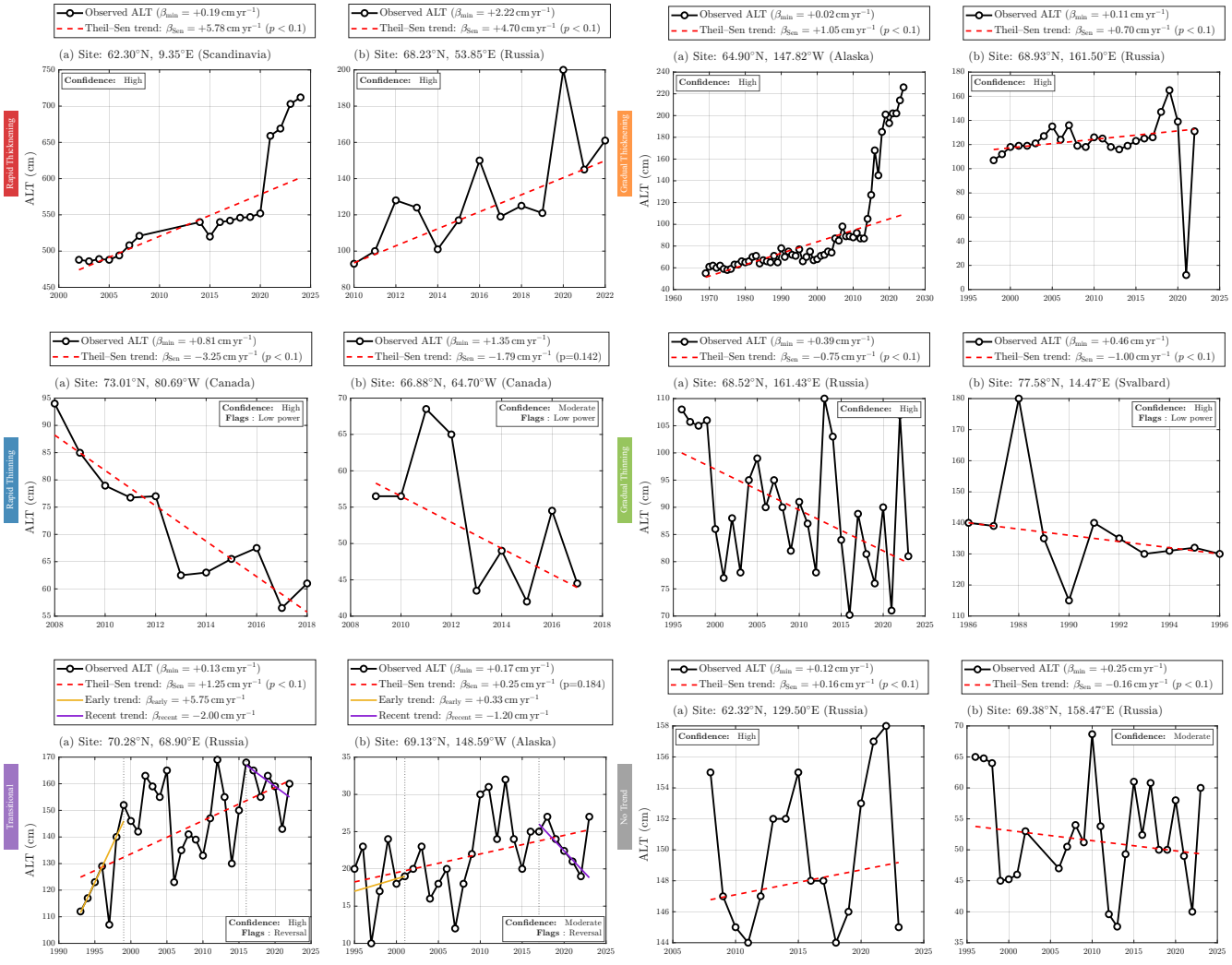

Figure 6. Representative ALT time series of sites assigned to the six ALDI classes. The red dashed line shows the full-period Theil–Sen slope estimate (β_{Sen}). For transitional sites, early and recent years' Sen slopes are additionally displayed to illustrate trajectory reversal and rate of change. Panel annotations report Mann–Kendall p-values, confidence levels, and diagnostic flags.

https://doi.org/10.5194/egusphere-2026-2639
Preprint. Discussion started: 2 June 2026

Thickening, and Rapid Thickening classes, with Thinning cases present but comparatively sparse. A similar pattern is observed across the Russian Arctic, where No Trend and Thickening classes are distributed across both the western and northeastern regions without forming a single geographically uniform cluster. The smaller groups of sites in Greenland, Iceland, and Scandinavia are also dominated by No Trend and Thickening classes, whereas Transitional sites remain rare and spatially isolated. However, Canada shows a more mixed class composition and stands out as it contains two of the three Rapid Thinning sites. The distribution of site-level Sen's slopes (see Fig. 5) corroborates these contrasts: regional means are positive everywhere except Canada, as the only region with a net Thinning pattern.

Individual slopes span from -3.25 to $+8.79\ \mathrm{cm\,yr^{-1}}$ across the sites. In addition, median slopes within each class are well separated (e.g., $+2.69\ \mathrm{cm\,yr^{-1}}$ for Rapid Thickening versus $\approx 0.00\ \mathrm{cm\,yr^{-1}}$ for No Trend versus $-1.80\ \mathrm{cm\,yr^{-1}}$ for Rapid Thinning), confirming that the empirically calibrated thresholds produce distinct categories. We note that although some of the most extreme thickening and thinning rates happen to occur in contrasting permafrost settings, no systematic relationship between permafrost zonation or ground-ice content and ALDI class emerges at the dataset level, as both factors contain most of the spectrum of the index types.

Representative time series for each class are shown in Fig. 6. The directional categories display the expected monotonic behaviour at rates consistent with their classification, while No Trend sites exhibit interannual fluctuations that dominate the underlying time series. The two Transitional sites merit specific attention: the Russian site (70.28 °N, 68.90° E) transitions from early thickening ($+5.75\ \mathrm{cm\,yr^{-1}}$) to recent thinning ($-2.00\ \mathrm{cm\,yr^{-1}}$), and the Alaskan site (69.13° N, 148.59° W) shows a more modest reversal from $+0.33$ to $-1.20\ \mathrm{cm\,yr^{-1}}$, which is a behaviour that the overall Sen's slope alone would not reveal. With the established spatial distribution and statistical characteristics of ALT trajectories across the Circum-Arctic CALM network, we now turn to identifying the environmental drivers of these dynamics through panel-data causal inference.

5.2 ALT Causal Inference

The causal analysis comprised 1704 site-year observations across 97 sites (constrained by ERA5-Land coastal coverage), stratified by ALDI category. The Rapid Thinning class was excluded due to insufficient data (29 obs. from 3 sites). We first estimated pooled effects across all sites to identify network-wide drivers, then stratified by ALDI class to assess how driver importance shifts with trajectory regime. The full raw coefficients, standard errors, confidence intervals, and p-values for all treatment-class combinations are provided in Table B1. The significant results are summarized visually in Fig. 7.

At the network level, thermal forcing seems to be the dominant control: TDD is the strongest pooled driver ($\hat{\beta}_{std} = 3.08$ cm in FE, 2.38 cm in FD; both $p < 0.001$), followed by FDD ($\hat{\beta}_{std} = -1.54$ cm, $p < 0.001$). Among non-thermal drivers, $\mathrm{P_{summer}}$ ($\hat{\beta}_{std} \approx 1.4$-$1.7$ cm), $\mathrm{NDVI_{summer}}$ ($\hat{\beta}_{std} = 2.28$ cm in FE), and SM ($\hat{\beta}_{std} = -1.15$ cm in FE) are significant, while NDWI and HWD showed weaker but detectable effects. Stratification by ALDI class revealed that these pooled signals mask substantial heterogeneity in driver importance across trajectory regimes.

Thermal sensitivity seem to scale monotonically with thickening intensity. TDD standardized effects decrease from 6.80 cm at Rapid Thickening sites through 4.85 cm at Gradual Thickening to 1.35 cm at No Trend sites, and are entirely absent at Gradual Thinning and Transitional sites. FDD follows a similar gradient. At Gradual Thickening sites, TDD is significant in

https://doi.org/10.5194/egusphere-2026-2639
Preprint. Discussion started: 2 June 2026

both FE and FD with comparable standardized magnitudes (4.85 vs. 4.77 cm). At Rapid Thickening sites, by contrast, TDD is significant only in FE.

For hydrological drivers, a complementary pattern is exhibited, gaining importance where thermal forcing weakened. For instance, P_{summer} is significant at No Trend and Transitional sites but absent at thickening sites, while SM and SDO appear only at Gradual Thickening sites. NDWI shows opposing signs across classes: strongly negative at Gradual Thinning sites ($\hat{\beta}_{std} = -2.65$ cm) but positive at Transitional sites ($\hat{\beta}_{std} \approx 1.0$-$1.3$ cm).

However, disturbance and vegetation signals seem to be class-specific. Specifically, $NDVI_{summer}$ seem to be robust across both specifications only at No Trend sites ($\hat{\beta}_{std} \approx 1.4$-$1.6$ cm), the sole class with consistent vegetation effects. ROS effects were negligible in the pooled analysis but emerge as a strong negative driver at Transitional ($\hat{\beta}_{std} \approx -3.2$ cm in both FE and FD) and Gradual Thinning sites ($\hat{\beta}_{std} = -4.94$ cm in FD). FireDays is significant only at Rapid Thickening sites ($\hat{\beta}_{std} = -1.05$ cm) and, with negligible standardized magnitude, at No Trend sites.

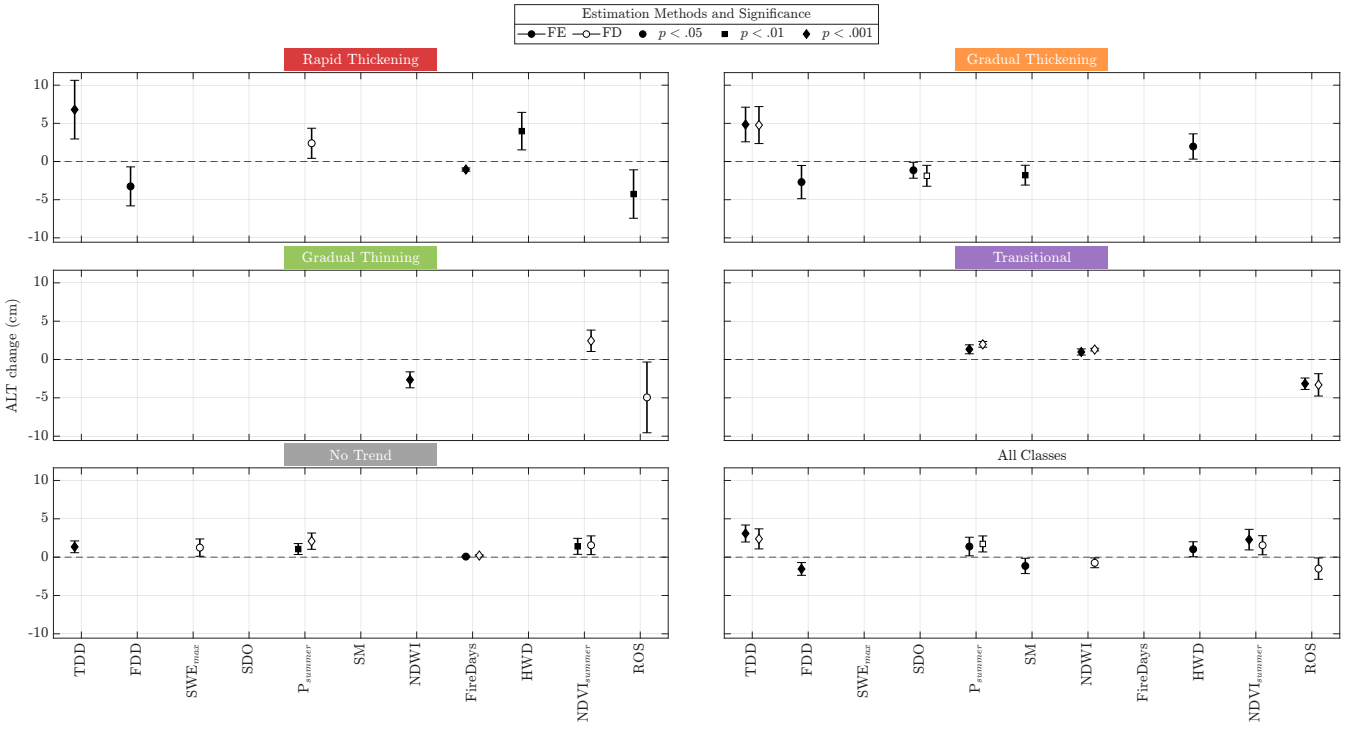

Figure 7. Standardized treatment effects ($\hat{\beta}_{std}$) on ALT, stratified by ALDI trajectory category. Points show estimated effects expressed as the change in ALT (cm) per one standard deviation increase in each treatment variable. The standardizing standard deviation matches the identifying variation of each estimator: within-site standard deviation for FE (filled markers) and standard deviation of first differences for FD (open markers). Horizontal lines indicate 95% confidence intervals. Marker shape denotes statistical significance (* $p < 0.05$, ** $p < 0.01$, *** $p < 0.001$). Only statistically significant estimates are displayed. Within-site SD is used for FE models; SD of first differences for FD models.

https://doi.org/10.5194/egusphere-2026-2639
Preprint. Discussion started: 2 June 2026

6 Discussion

This study combines a trajectory-based classification of active layer thickness (ALT) dynamics with panel-data causal inference to provide a process-oriented interpretation of permafrost change across the CALM network. The ALDI framework reveals a Circum-Arctic system dominated by thickening (3.5:1 thickening-to-thinning ratio), yet characterized by substantial regional and site-level heterogeneity, including rare but important trajectory reversals. While pooled causal estimates suggest a primarily thermally driven system, stratification by trajectory class demonstrates that the controls on ALT are not uniform but shift systematically across regimes. Specifically, thermal forcing dominates at thickening sites, whereas hydrological and disturbance-related processes become increasingly important at thinning and transitional sites. The divergence between FE and FD estimates further indicates that these controls operate on distinct temporal scales, distinguishing persistent structural influences from interannual variability. Together, these results point to a dynamic, regime-dependent system in which the drivers of ALT dynamics evolve alongside the trajectory of permafrost change itself.

6.1 Thickening dominance and regional heterogeneity

The 3.5:1 thickening-to-thinning ratio observed here is broadly consistent with multi-decadal observations of increasing active layer thickness (ALT) across the Arctic. Long-term CALM records and hemispheric syntheses have repeatedly documented widespread ALT deepening associated with atmospheric thermal shifting and increased ground heat flux (Streletskiy et al., 2017; Shiklomanov et al., 2012b; Luo et al., 2016). This pattern aligns with evidence of large-scale permafrost thaw reported from borehole networks and observational syntheses, which indicate increasing ground temperatures across both continuous and discontinuous permafrost zones (Biskaborn et al., 2019a; Romanovsky et al., 2010; Smith et al., 2010). Early observational work in Alaska already highlighted that sustained thermal shifts lead to progressive active layer deepening through enhanced summer energy input (Osterkamp, 2007), a process that remains evident in the present dataset.

At the same time, the CALM network itself, designed to capture spatial variability in ALT dynamics (Brown et al., 2000), reveals substantial heterogeneity in response. Canada stands out here as the sole region with net thinning, consistent with recent observations of localized permafrost degradation accompanied by thaw subsidence and surface lowering in northwest Canada (O'Neill et al., 2023). Such thinning does not contradict overall thermal trends but instead reflects geomorphological responses (e.g., ground-ice melt and subsidence) that can reduce measured ALT even under shifting conditions. The absence of a systematic relationship between permafrost zonation or ground-ice content and ALDI class further supports the interpretation that ALT trajectories are emergent outcomes of interacting local processes rather than deterministic functions of large-scale permafrost classification.

6.2 Driver regime shifts across trajectory classes

The monotonic decline in thermal sensitivity across trajectory classes (Fig. 7) is consistent with a transition from thermally dominated to process-limited regimes of ALT evolution. Under the classical Stefan equation, thaw depth scales with cumulative summer warmth, assuming efficient energy transfer into the ground (Zhang, 2005). This assumption appears valid for Rapid

https://doi.org/10.5194/egusphere-2026-2639
Preprint. Discussion started: 2 June 2026

and Gradual Thickening sites, where thawing degree days (TDD) exert strong and consistent effects. Similar strong coupling between air temperature and ALT has been reported in observational studies where the thawing n-factor, which is the ratio of seasonal degree-day sum at the soil surface to that in the air at standard screen height, efficiently translates atmospheric forcing into ground response (Klene et al., 2001).

However, numerous field studies have shown that this coupling weakens under increasing ecological and hydrological complexity. Organic layer thickening, vegetation expansion, snow insulation and melt timing, and latent heat effects associated with soil moisture all act to buffer heat transfer (Romanovsky and Osterkamp, 1997; Shiklomanov et al., 2010). The disappearance of thermal drivers in thinning and transitional classes is therefore physically consistent with a shift toward edaphic and hydrological control. This interpretation is further supported by studies showing that moisture-controlled landscapes can exhibit decadal variability in ALT independent of temperature trends due to changes in soil thermal properties and drainage conditions (Shiklomanov et al., 2010).

Hydrological controls emerging in the weaker thermal regimes are also well grounded in prior literature. Soil moisture influences thermal conductivity and latent heat consumption, thereby modulating thaw penetration (Romanovsky and Osterkamp, 1997). The observed significance of SDO at Gradual Thickening sites aligns with evidence that earlier snowmelt extends the thaw season, enhancing cumulative ground heat input. The sign reversal of NDWI across trajectory classes suggests a mechanistic shift also noted in field-based studies: surface water can either dampen thaw through thermal buffering or accelerate degradation through thermokarst processes and landscape instability (Jorgenson et al., 2006). Such dual roles of water are increasingly recognized in studies of permafrost degradation, particularly in ice-rich terrains where hydrological reorganization accompanies thaw.

Disturbance-related processes further reinforce the importance of regime-specific dynamics. ROS events and wildfire activity are known to alter surface energy balance, vegetation cover, and insulation properties, thereby influencing ALT evolution. Their absence in pooled estimates but emergence under stratification highlights a key limitation of network-wide analyses: averaging across heterogeneous regimes can obscure physically meaningful signals. This finding echoes broader concerns in permafrost research that aggregated analyses may mask nonlinear and site-specific responses to forcing of environmental parameters.

6.3 Structural versus interannual sensitivity

The divergence between FE and FD estimates provides additional insight into the temporal structure of ALT response. FE estimates capture persistent within-site associations, while FD estimates isolate interannual variability. The resulting patterns align with known permafrost processes.

At Gradual Thickening sites, the agreement between FE and FD for thermal drivers indicates that both long-term trends and year-to-year variability are governed by atmospheric forcing. This is consistent with sites where ground thermal regimes remain closely coupled to long-term weather patterns. In contrast, Rapid Thickening sites show significance only in FE estimates, suggesting that ALT deepening reflects cumulative thermal forcing and long-term energy imbalance rather than short-term fluctuations. This behavior is consistent with progressive permafrost thermal shifts observed in borehole records, where thermal inertia and latent heat effects dampen interannual variability (Biskaborn et al., 2019a).

https://doi.org/10.5194/egusphere-2026-2639
Preprint. Discussion started: 2 June 2026

Transitional sites, where FE and FD estimates agree for hydrological drivers, appear to represent actively evolving systems undergoing regime change. Such agreement indicates that both structural conditions and interannual variability are controlled by the same processes, consistent with landscapes experiencing ongoing thermokarst development or drainage reorganization. This interpretation aligns with recent observations of rapid landscape change in degrading permafrost regions, where hydrological and geomorphological processes dominate system dynamics (O'Neill et al., 2023).

6.4 Implications for permafrost system dynamics

Taken together, the results point to a conceptual model in which ALT dynamics evolve through distinct driver regimes. Early-stage or stable permafrost systems are primarily temperature-controlled, with ALT responding predictably to atmospheric forcing. As degradation progresses, feedbacks involving soil moisture, vegetation, and disturbance processes increasingly modulate or even dominate the response. This transition has been noted in both observational and modeling studies, which emphasize that permafrost responses to enviromental conditions is inherently nonlinear and mediated by local conditions (Luo et al., 2016; Biskaborn et al., 2019b).

The identification of trajectory-dependent driver regimes therefore provides a framework for reconciling apparently conflicting observations in the literature. For example, strong temperature–ALT relationships reported in some regions coexist with weak or absent relationships in others because sites occupy different positions along this trajectory continuum. By explicitly accounting for trajectory class, the ALDI framework helps unify these observations into a coherent process-based interpretation.

6.5 Limitations and outlook

Several limitations of the present analysis warrant discussion. The ERA5-Land reanalysis excludes grid cells classified as ocean under its land-sea mask, which at Arctic latitudes misclassifies many coastal sites. This filtering removed 32 of 129 CALM sites from the causal analysis, disproportionately affecting high-latitude coastal locations where maritime influences on permafrost thermal regimes may differ from inland sites. Given that coastal permafrost often exhibits distinct thermal and hydrological behavior, this exclusion may bias the inferred driver relationships.

The CALM network itself, while uniquely valuable for long-term monitoring, reflects uneven spatial coverage (Brown et al., 2000). Alaska and Russia are overrepresented relative to regions such as Scandinavia and the Canadian Archipelago, and site characteristics are not uniformly distributed across environmental gradients. As a result, the driver estimates reported here should be interpreted as conditional on the existing monitoring network.

The small sample size of certain trajectory classes, particularly Transitional and Rapid Thinning sites, limits statistical generalizability. However, the consistency of their mechanistic signals suggests that they represent meaningful system states rather than statistical artifacts. Expanding observations in these underrepresented regimes—particularly in areas experiencing rapid thermokarst or subsidence—would be a valuable priority.

Methodologically, the fixed-effects design controls for time-invariant confounders but cannot fully address time-varying unobserved processes such as organic layer degradation, vegetation shifts, or evolving drainage patterns. These processes are

https://doi.org/10.5194/egusphere-2026-2639
Preprint. Discussion started: 2 June 2026

known to play critical roles in permafrost dynamics and may introduce bias if not explicitly modeled. Future work could incorporate additional robustness checks, including placebo tests, sensitivity analyses, or causal frameworks that explicitly model dynamic confounding.

Finally, the assumption of linear marginal effects may not hold near critical thresholds, particularly in ice-rich permafrost approaching 0°C, where phase-change dynamics can produce abrupt transitions. Incorporating nonlinear or threshold-based models would be a valuable extension of the present framework.

Looking forward, the driver regime shifts identified here have important implications for permafrost projections. Earth system models that rely primarily on temperature-based parameterizations may fail to capture the increasing importance of hydrological and disturbance processes as degradation progresses. It is also important to take into consideration the local change in surface conditions such as altered drainage or ponding, surface disturbance and recovery, or increased organic insulation that weakens air-to-ground coupling, which may prevent increase in thaw depth. The ALDI framework offers a pathway for addressing this limitation by enabling trajectory-aware evaluation of model performance. Applying ALDI classification over moving time windows could also provide an early-warning indicator of regime shifts, allowing detection of emerging transitions before they manifest as long-term trends.

7 Conclusions

This study introduced ALDI, a trajectory-based classification framework that partitions CALM network sites into six classes based on the direction, rate, and temporal structure of ALT change. Applied to 129 circum-Arctic sites, ALDI reveals a system dominated by thickening (3.5:1 thickening-to-thinning ratio) but marked by pronounced regional heterogeneity and the presence of rare yet informative trajectory reversals. When coupled with panel-data causal inference, the results demonstrate that the drivers of ALT change are not spatially uniform but vary systematically with trajectory regime: thickening sites are primarily governed by thermal forcing, whereas thinning and transitional sites are increasingly influenced by hydrological and disturbance-related processes, relationships that are obscured in pooled network-wide analyses. This regime-dependent structure underscores the complexity of active layer dynamics and highlights the limitations of treating permafrost response as uniformly temperature-driven.

However, due to to data availability limitations, future work should prioritize expanding spatial coverage beyond the current site network and incorporate higher-resolution surface condition data (e.g., hydrology, vegetation structure, and disturbance history) to reduce geographic sampling biases and better capture underrepresented permafrost regions. Additionally, improving temporal continuity and consistency of observations would help address data gaps and uncertainties in trajectory classification. Looking forward, applying ALDI over moving time windows offers a pathway for detecting emerging regime shifts, while evaluating whether Earth system models reproduce these class-dependent driver patterns provides a physically grounded benchmark for improving projections of permafrost change under shifting environmental conditions within the Arctic region.

https://doi.org/10.5194/egusphere-2026-2639
Preprint. Discussion started: 2 June 2026

Funding

This material is based upon work supported by the Broad Agency Announcement Program and the Cold Regions Research and Engineering Laboratory (ERDC-CRREL) under Contract W913E524C0017.

Data Availability

All data and scripts used in this manuscript are openly available on Zenodo (Ahajjam, 2026). The dataset can be accessed at https://doi.org/10.5281/zenodo.20497762 .

Acknowledgments

DISTRIBUTION A: Approved for Public Release. Distribution is Unlimited. This material is based upon work supported by the Broad Agency Announcement Program and the Cold Regions Research and Engineering Laboratory (ERDC-CRREL) under Contract No. W913E524C0017. Special thanks to Dr. Dmitry Nicolsky and Dr Vladimir Romanovsky of the University of Alaska Fairbanks Geophysical Institute Permafrost Laboratory.

https://doi.org/10.5194/egusphere-2026-2639
Preprint. Discussion started: 2 June 2026

Appendix A: ALDI classification results

Table A1: Per-site ALDI classification results for all 129 CALM sites. Sites are grouped by ALDI class and sorted by descending Sen's slope within each group. ALDI classes: Rapid Thickening (RT), Gradual Thickening (GT), No Trend (NT), Gradual Thinning (GTh), Rapid Thinning (RTh), Transitional (Tr); Confidence: High (H), Moderate (M), Low (L); Flags: Mann-Kendall significant at $\alpha = 0.10$ (S), low statistical power (LP), trajectory reversal detected (R). All slopes are in $\mathrm{cm\,yr^{-1}}$.

Lat (°)	Lon (°)	n	Period	$\overline{\mathrm{ALT}}$ (cm)	Class	β_{Sen} $\mathrm{cm\,yr^{-1}}$	95 % CI $\mathrm{cm\,yr^{-1}}$	p_{MK}	Confidence	Flags
64.71	-148.15	34	1990-2024	156.2	RT	+8.79	[+1.67, +17.90]	0.050	H	S
62.30	9.35	17	2002-2024	555.8	RT	+5.78	[+3.17, +12.00]	0.035	H	S
66.71	66.57	9	2013-2021	135.6	RT	+5.19	[+0.33, +9.75]	0.118	H	S, LP
68.23	53.85	13	2010-2022	129.5	RT	+4.70	[+0.20, +7.10]	0.042	H	S
77.53	14.49	9	1987-1996	139.1	RT	+4.44	[-10.36, +15.00]	0.369	M	LP
77.57	14.47	10	1986-1996	144.0	RT	+4.00	[-0.86, +10.00]	0.138	M	LP
77.54	14.49	9	1987-1996	123.7	RT	+3.75	[-11.75, +22.50]	0.403	M	LP
67.48	76.70	14	2008-2022	130.1	RT	+3.29	[+1.25, +6.67]	0.113	H	S
64.88	-147.67	19	2005-2023	100.4	RT	+3.06	[+1.00, +6.00]	0.045	H	S
66.70	66.36	9	2013-2021	147.9	RT	+2.90	[-9.20, +12.50]	0.598	L	LP
70.30	68.88	16	2007-2022	104.5	RT	+2.88	[+0.00, +4.25]	0.080	H	S
77.54	14.53	11	1986-1998	124.3	RT	+2.69	[-0.50, +3.67]	0.088	H	S
64.92	-125.58	9	1988-1996	77.5	RT	+2.35	[+0.76, +4.48]	0.048	H	S, LP
68.70	161.55	15	2003-2017	109.7	RT	+2.33	[-3.25, +4.90]	0.071	H	S
77.56	14.58	10	1987-1998	152.1	RT	+2.33	[-0.77, +5.49]	0.274	M	-
69.89	-142.98	15	2001-2015	47.9	RT	+1.89	[+0.00, +3.62]	0.103	M	-
67.48	86.43	15	2008-2023	161.4	RT	+1.84	[+1.33, +5.00]	0.084	H	S
77.56	14.43	11	1986-1998	122.2	RT	+1.74	[-2.88, +5.00]	0.246	M	-
65.54	-171.63	15	2010-2024	99.8	RT	+1.62	[+0.67, +2.92]	0.118	H	S
67.58	64.18	28	1996-2023	120.9	RT	+1.61	[+1.00, +1.83]	0.046	H	S
78.18	16.47	27	1998-2024	178.5	RT	+1.58	[+0.86, +1.75]	0.048	H	S
77.58	14.45	10	1986-1996	127.6	RT	+1.43	[-0.43, +2.80]	0.124	M	LP
70.30	68.84	16	2007-2022	138.1	RT	+1.40	[-2.60, +5.00]	0.147	M	-
68.73	158.90	17	2007-2023	85.6	GT	+1.22	[+0.00, +3.00]	0.066	H	S

Continued on next page

https://doi.org/10.5194/egusphere-2026-2639
Preprint. Discussion started: 2 June 2026

Table A1 continued

Lat (°)	**Lon** (°)	n	**Period**	$\overline{\text{ALT}}$ (cm)	**Class**	β_{Sen} cm yr^{-1}	95 % CI cm yr^{-1}	p_{MK}	**Confidence**	**Flags**
61.68	8.37	25	1999-2024	228.2	GT	+1.11	[-0.41, +1.60]	0.081	H	S
77.55	14.49	9	1987-1996	152.2	GT	+1.11	[-14.00, +11.00]	0.864	L	LP
64.90	-147.82	56	1969-2024	92.7	GT	+1.05	[+0.62, +3.00]	0.005	H	S
74.47	-20.56	29	1996-2024	102.8	GT	+1.02	[+0.25, +1.77]	0.043	H	S
77.55	14.50	10	1986-1996	129.6	GT	+1.00	[-0.60, +2.50]	0.257	M	LP
64.84	-163.72	15	2008-2023	121.6	GT	+0.95	[-0.38, +3.40]	0.069	H	S
70.20	-161.08	19	1998-2016	52.8	GT	+0.93	[-0.38, +2.50]	0.221	M	-
70.27	68.89	9	2014-2022	59.7	GT	+0.83	[-2.00, +5.00]	0.529	L	LP
62.70	-123.06	8	2001-2008	125.0	GT	+0.71	[+0.00, +3.33]	0.112	L	LP
68.93	161.50	25	1998-2022	121.1	GT	+0.70	[-0.50, +1.92]	0.024	H	S
68.33	18.83	46	1978-2023	110.0	GT	+0.68	[-0.37, +1.38]	0.075	H	S
68.61	-149.31	29	1995-2023	78.7	GT	+0.68	[+0.00, +1.89]	0.193	M	-
74.47	-20.55	29	1996-2024	90.2	GT	+0.67	[+0.29, +1.19]	0.044	H	S
65.45	-164.63	15	2008-2023	103.5	GT	+0.64	[-1.33, +1.50]	0.215	L	-
77.58	14.47	10	1986-1996	118.5	GT	+0.62	[-2.50, +5.00]	0.646	L	LP
62.01	129.66	16	2008-2023	222.2	GT	+0.61	[+0.25, +1.00]	0.089	H	S
81.40	-76.71	20	1999-2018	73.7	GT	+0.58	[+0.18, +1.01]	0.078	H	S
78.20	15.84	21	2000-2020	116.1	GT	+0.55	[+0.00, +1.33]	0.176	M	-
69.50	-148.56	28	1996-2023	98.2	GT	+0.51	[+0.20, +1.00]	0.118	H	S
66.45	-150.62	25	1996-2024	55.8	GT	+0.50	[+0.17, +0.62]	0.070	H	S
67.80	-134.13	10	1998-2008	111.0	GT	+0.50	[-1.00, +1.51]	0.411	L	LP
68.80	160.95	26	1996-2023	128.1	GT	+0.50	[-1.26, +1.67]	0.189	L	-
68.83	161.03	27	1996-2023	139.1	GT	+0.50	[-0.80, +1.76]	0.205	M	-
70.86	-153.91	19	1998-2016	39.3	GT	+0.50	[+0.29, +1.13]	0.109	H	S
70.57	-152.97	13	2004-2016	31.5	GT	+0.48	[-1.25, +1.47]	0.435	M	-
70.45	-157.40	29	1995-2023	116.5	GT	+0.44	[+0.00, +1.65]	0.281	L	-
69.08	158.90	22	1996-2023	79.3	GT	+0.44	[-1.50, +2.38]	0.334	M	-
64.78	176.97	30	1994-2023	64.3	GT	+0.40	[+0.00, +0.98]	0.152	M	-
69.15	-148.85	22	1996-2022	63.8	GT	+0.38	[-0.09, +1.00]	0.125	M	-
77.56	14.49	11	1986-1998	162.5	GT	+0.37	[-1.67, +3.75]	0.714	L	-

Continued on next page

https://doi.org/10.5194/egusphere-2026-2639
Preprint. Discussion started: 2 June 2026

Table A1 continued

Lat (°)	**Lon** (°)	n	**Period**	$\overline{\text{ALT}}$ (cm)	**Class**	β_{Sen} cm yr^{-1}	95 % CI cm yr^{-1}	p_{MK}	**Confidence**	**Flags**
64.57	177.20	27	1996-2023	88.0	GT	+0.36	[-0.56, +1.26]	0.091	H	S
70.16	-148.47	24	1996-2022	85.9	GT	+0.36	[+0.00, +0.75]	0.160	M	-
71.79	71.42	19	2004-2023	52.3	GT	+0.34	[-1.29, +1.36]	0.535	M	-
68.07	-149.58	23	1996-2022	59.1	GT	+0.33	[+0.09, +0.86]	0.099	H	S
65.60	-171.05	25	2000-2024	100.7	GT	+0.30	[+0.02, +0.75]	0.216	H	S
70.37	-148.57	28	1995-2023	94.1	NT	+0.30	[-0.42, +1.06]	0.312	M	-
70.28	68.89	16	2007-2022	104.7	NT	+0.29	[-1.46, +2.51]	0.543	L	-
70.63	-156.84	11	2004-2014	41.1	NT	+0.29	[-0.12, +0.79]	0.450	M	LP
70.28	-148.92	28	1995-2023	56.8	NT	+0.25	[+0.00, +1.00]	0.265	M	-
68.62	-149.61	29	1995-2023	81.8	NT	+0.22	[-0.09, +0.60]	0.225	M	-
65.17	-147.90	50	1972-2024	61.9	NT	+0.20	[+0.00, +0.33]	0.125	M	-
71.79	129.42	21	2001-2023	45.5	NT	+0.19	[-2.73, +2.00]	0.479	M	-
62.32	129.50	16	2008-2023	149.8	NT	+0.16	[-0.83, +1.51]	0.015	H	S
70.28	-148.87	28	1995-2023	107.6	NT	+0.12	[+0.00, +1.24]	0.259	L	-
77.57	14.45	10	1986-1996	112.5	NT	+0.12	[-3.50, +3.45]	1.000	L	LP
68.48	-155.73	18	2000-2022	96.2	NT	+0.11	[-0.57, +1.53]	0.816	L	-
69.72	-134.46	10	1998-2008	74.5	NT	+0.11	[-2.25, +2.10]	0.942	L	LP
77.53	14.49	11	1986-1998	164.0	NT	+0.11	[-2.88, +3.00]	0.666	L	-
68.48	-149.50	23	1996-2022	79.4	NT	+0.08	[-0.43, +1.03]	0.702	L	-
70.34	-152.05	19	1998-2016	29.9	NT	+0.08	[-0.17, +0.50]	0.127	M	-
69.48	156.98	19	1996-2021	61.3	NT	+0.08	[-0.00, +0.38]	0.299	L	-
69.44	-148.67	29	1995-2023	85.0	NT	+0.07	[-0.33, +0.93]	0.708	M	-
69.85	159.50	22	1999-2023	67.6	NT	+0.06	[-1.56, +1.25]	0.852	L	-
70.55	147.43	16	2004-2021	68.5	NT	+0.06	[-0.67, +0.51]	0.801	L	-
69.17	154.43	19	2005-2023	72.2	NT	+0.03	[-0.85, +0.62]	0.956	L	-
69.32	154.98	22	1998-2023	76.1	NT	+0.02	[-0.71, +0.60]	0.844	L	-
61.89	-121.60	10	1999-2008	124.0	NT	+0.00	[+0.00, +2.00]	0.092	M	S, LP
64.78	-141.11	10	2009-2019	88.4	NT	+0.00	[-2.00, +5.00]	0.670	L	LP
65.31	72.86	26	1997-2022	201.5	NT	+0.00	[+0.00, +0.83]	0.178	L	-
65.66	-149.08	8	2009-2016	82.9	NT	+0.00	[-4.00, +2.50]	1.000	L	LP

Continued on next page

https://doi.org/10.5194/egusphere-2026-2639
Preprint. Discussion started: 2 June 2026

Table A1 continued

Lat (°)	**Lon** (°)	n	**Period**	$\overline{\text{ALT}}$ (cm)	**Class**	β_{Sen} cm yr^{-1}	95 % CI cm yr^{-1}	p_{MK}	**Confidence**	**Flags**
66.31	76.90	15	2008-2022	181.4	NT	+0.00	[-1.96, +4.25]	0.630	L	-
66.72	66.08	8	2016-2023	197.1	NT	+0.00	[-2.43, +0.00]	0.188	L	LP
67.07	62.93	12	2012-2023	144.6	NT	+0.00	[-4.40, +4.00]	0.778	L	-
67.33	63.73	24	1998-2022	199.2	NT	+0.00	[-0.29, +0.00]	0.218	L	-
68.68	-134.15	8	2000-2008	130.3	NT	+0.00	[+0.00, +0.00]	0.561	L	LP
68.82	161.00	26	1996-2023	78.6	NT	+0.00	[-1.40, +0.55]	0.946	L	-
69.43	88.47	19	2005-2023	155.0	NT	+0.00	[+0.00, +0.62]	0.143	L	-
69.67	-148.72	26	1996-2022	102.1	NT	+0.00	[-0.98, +1.14]	0.881	L	-
69.72	66.75	29	1995-2023	173.0	NT	+0.00	[-0.40, +1.43]	0.984	L	-
69.75	-154.62	18	1999-2016	119.2	NT	+0.00	[+0.00, +0.00]	0.177	L	-
70.08	159.58	23	1999-2023	57.4	NT	+0.00	[-1.20, +0.50]	1.000	L	-
70.28	-148.89	28	1995-2023	67.7	NT	+0.00	[-0.50, +0.40]	0.796	L	-
71.32	-156.60	40	1962-2023	65.2	NT	+0.00	[-0.18, +0.30]	0.846	L	-
77.54	14.51	11	1986-1998	92.7	NT	+0.00	[-3.67, +3.00]	1.000	L	-
77.56	14.55	11	1986-1998	69.0	NT	+0.00	[-1.71, +0.78]	1.000	L	-
77.58	14.45	10	1986-1996	120.8	NT	+0.00	[-4.00, +3.67]	0.809	L	LP
68.74	161.50	20	2003-2022	127.3	NT	-0.03	[-4.00, +1.67]	0.692	L	-
69.37	-134.95	11	1998-2008	130.0	NT	-0.06	[-0.50, +0.00]	0.119	L	LP
69.40	-152.14	19	1998-2016	36.1	NT	-0.07	[-0.29, +1.00]	0.697	L	-
69.78	-144.79	12	2002-2016	50.2	NT	-0.14	[-3.57, +5.00]	0.834	L	-
70.08	159.92	22	2000-2023	64.2	NT	-0.15	[-2.00, +1.10]	0.585	L	-
69.38	158.47	20	1996-2023	52.6	NT	-0.16	[-0.47, +0.50]	0.076	M	S
68.72	161.53	11	2003-2016	176.9	NT	-0.17	[-1.25, +0.93]	0.821	L	-
69.38	158.47	18	1999-2023	57.5	NT	-0.21	[-1.21, +0.25]	0.471	M	-
70.04	-157.08	13	2004-2016	48.8	NT	-0.21	[-1.43, +1.88]	0.792	M	-
77.55	14.47	10	1986-1996	127.5	NT	-0.22	[-2.14, +2.50]	0.830	L	LP
64.63	176.97	14	2010-2023	79.0	GTh	-0.33	[-1.50, +0.25]	0.267	L	-
65.28	-126.88	8	1989-1996	95.2	GTh	-0.36	[-26.49, +33.31]	1.000	L	LP
69.99	-153.09	19	1998-2016	43.2	GTh	-0.38	[-0.75, +0.29]	0.076	H	S
69.22	-134.29	11	1998-2008	89.9	GTh	-0.50	[-3.13, +1.75]	0.661	M	LP

Continued on next page

https://doi.org/10.5194/egusphere-2026-2639
Preprint. Discussion started: 2 June 2026

Table A1 continued

Lat (°)	**Lon** (°)	n	**Period**	$\overline{\text{ALT}}$ (cm)	**Class**	β_{Sen} cm yr^{-1}	95 % CI cm yr^{-1}	p_{MK}	**Confidence**	**Flags**
77.55	14.49	10	1986-1996	114.4	GTh	-0.67	[-2.67, +1.23]	0.232	L	LP
68.30	54.50	19	1999-2019	139.2	GTh	-0.68	[-2.00, +1.26]	0.266	M	-
68.52	161.43	27	1996-2023	90.1	GTh	-0.75	[-1.23, +0.09]	0.037	H	S
72.81	-79.33	9	2009-2018	59.9	GTh	-0.75	[-1.88, -0.25]	0.067	H	S, LP
77.56	14.52	10	1987-1998	177.2	GTh	-0.89	[-6.00, +5.00]	0.274	L	-
77.56	14.46	11	1986-1998	158.5	GTh	-0.99	[-4.65, +3.12]	0.827	M	-
77.53	14.48	10	1986-1996	98.2	GTh	-1.00	[-7.00, +3.50]	0.711	L	LP
77.58	14.47	10	1986-1996	137.0	GTh	-1.00	[-5.00, +0.00]	0.064	H	S, LP
65.19	-126.47	11	1998-2008	94.4	GTh	-1.05	[-3.50, +2.01]	0.579	M	LP
68.74	161.39	20	2003-2022	93.6	GTh	-1.25	[-4.80, -0.25]	0.115	H	S
77.54	14.55	11	1986-1998	164.0	RTh	-1.53	[-6.10, +1.67]	0.290	M	-
66.88	-64.70	9	2009-2017	53.3	RTh	-1.79	[-6.50, +0.00]	0.142	M	LP
73.01	-80.69	9	2008-2018	71.6	RTh	-3.25	[-4.58, -1.50]	0.067	H	S, LP
70.28	68.90	29	1993-2022	144.8	Tr	+1.25	[+0.00, +2.00]	0.051	H	S, R
69.13	-148.59	27	1995-2023	21.8	Tr	+0.25	[+0.00, +0.67]	0.184	M	R

https://doi.org/10.5194/egusphere-2026-2639
Preprint. Discussion started: 2 June 2026

Appendix B: ALDI Causal inference

Table B1: Causal effect estimates of environmental drivers on ALT, stratified by ALDI trajectory class. Effects are estimated using site fixed-effects with cluster-robust FE and FD. For each treatment-class combination, the raw effect estimate ($\hat{\beta}$; cm ALT per unit treatment), standard error (SE), standardized effect ($\hat{\beta}_{std} = \hat{\beta} \times \sigma_X$; cm ALT per one standard deviation (SD) increase in treatment), the standardizing SD (σ_X; within-site SD for FE, SD of first differences for FD), 95% confidence interval bounds on the raw effect, p-value, number of site-year observations (N), and number of unique CALM sites. Significance levels: $^{*}p < 0.05$, $^{**}p < 0.01$, $^{***}p < 0.001$. The 'All' class pools all sites regardless of trajectory. The Rapid Thinning class was excluded due to insufficient sample size (29 obs. from 3 sites). ALDI classes: Rapid Thickening (RT), Gradual Thickening (GT), No Trend (NT), Gradual Thinning (GTh), Rapid Thinning (RTh), Transitional (Tr)

Method	Class	Treatm.	Effect	SE	Effect Std	SD Treatm.	CI_{Lower}	CI_{Upper}	p	N	Sites
FE	All	TDD	0.023	0.004	3.083	135.907	0.015	0.031	0.000	1704	97
		FDD	-0.004	0.001	-1.540	384.334	-0.006	-0.002	0.000	1704	97
		SWE_{max}	6.919	8.774	0.308	0.044	-10.277	24.115	0.430	1704	97
		SDO	-0.094	0.084	-0.579	6.167	-0.259	0.071	0.264	1704	97
		P_{summer}	0.032	0.014	1.383	43.114	0.004	0.060	0.026	1704	97
		SM	-54.877	24.373	-1.146	0.021	-102.646	-7.108	0.024	1594	89
		NDWI	1.011	6.678	0.085	0.084	-12.078	14.101	0.880	2064	119
		FireDays	-2.502	5.025	-0.107	0.043	-12.350	7.346	0.619	1254	74
		HWD	0.193	0.093	1.029	5.338	0.010	0.376	0.039	1704	97
		$NDVI_{summer}$	58.560	17.558	2.285	0.039	24.147	92.973	0.001	1201	71
		ROS	-0.566	0.401	-0.876	1.547	-1.351	0.219	0.158	1704	97
	RT	TDD	0.046	0.013	6.796	146.953	0.020	0.072	0.001	252	18
		FDD	-0.008	0.003	-3.252	406.053	-0.014	-0.002	0.013	252	18
		SWE_{max}	12.544	12.555	0.899	0.072	-12.063	37.152	0.318	252	18
		SDO	-0.287	0.369	-1.924	6.707	-1.011	0.437	0.437	252	18
		P_{summer}	0.092	0.077	4.241	45.925	-0.059	0.244	0.232	252	18
		SM	-216.982	198.524	-2.975	0.014	-606.081	172.118	0.274	219	15
		NDWI	38.165	23.955	3.464	0.091	-8.785	85.115	0.111	297	20
		FireDays	-27.356	2.798	-1.050	0.038	-32.840	-21.872	0.000	174	11
		HWD	0.611	0.192	3.983	6.521	0.234	0.988	0.001	252	18
		$NDVI_{summer}$	244.759	129.462	7.684	0.031	-8.982	498.501	0.059	161	10

https://doi.org/10.5194/egusphere-2026-2639
Preprint. Discussion started: 2 June 2026

Table B1 continued

Method	Class	Treatm.	Effect	SE	Effect Std	SD Treatm.	CI_{Lower}	CI_{Upper}	p	N	Sites
		ROS	-2.016	0.766	-4.258	2.112	-3.518	-0.514	0.009	252	18
	GT	TDD	0.038	0.009	4.849	128.087	0.020	0.056	0.000	425	21
		FDD	-0.008	0.003	-2.693	345.269	-0.014	-0.002	0.015	425	21
		SWE_{max}	3.475	19.208	0.150	0.043	-34.172	41.122	0.856	425	21
		SDO	-0.212	0.099	-1.140	5.375	-0.407	-0.018	0.032	425	21
		P_{summer}	0.012	0.016	0.536	45.108	-0.019	0.042	0.444	425	21
		SM	-92.062	34.181	-1.785	0.019	-159.056	-25.068	0.007	408	20
		NDWI	-2.636	11.017	-0.232	0.088	-24.228	18.956	0.811	689	34
		FireDays	0.000	0.000		0.000	0.000	0.000	0.000	329	18
		HWD	0.525	0.225	1.970	3.755	0.084	0.965	0.020	425	21
		$NDVI_{summer}$	46.278	24.311	2.102	0.045	-1.370	93.927	0.057	312	17
		ROS	0.736	0.541	1.177	1.599	-0.323	1.796	0.173	425	21
	NT	TDD	0.010	0.003	1.347	138.414	0.004	0.015	0.001	791	41
		FDD	-0.001	0.001	-0.585	394.401	-0.003	0.000	0.069	791	41
		SWE_{max}	1.792	13.630	0.064	0.036	-24.923	28.506	0.895	791	41
		SDO	-0.005	0.059	-0.032	6.616	-0.120	0.110	0.934	791	41
		P_{summer}	0.025	0.009	1.056	42.144	0.008	0.042	0.004	791	41
		SM	-17.544	21.484	-0.413	0.024	-59.652	24.564	0.414	741	38
		NDWI	-2.197	4.101	-0.160	0.073	-10.235	5.841	0.592	843	48
		FireDays	1.209	0.509	0.070	0.058	0.212	2.207	0.017	608	35
		HWD	-0.020	0.066	-0.111	5.692	-0.149	0.110	0.768	791	41
		$NDVI_{summer}$	36.206	13.705	1.408	0.039	9.345	63.067	0.008	585	34
		ROS	-0.151	0.462	-0.187	1.239	-1.056	0.755	0.744	791	41
	GTh	TDD	-0.003	0.010	-0.363	121.558	-0.023	0.017	0.774	151	12
		FDD	0.001	0.005	0.431	343.272	-0.009	0.011	0.809	151	12
		SWE_{max}	22.673	37.598	0.836	0.037	-51.018	96.364	0.546	151	12
		SDO	0.216	0.368	1.113	5.154	-0.506	0.938	0.558	151	12
		P_{summer}	0.022	0.032	0.724	33.219	-0.040	0.084	0.490	151	12
		SM	9.766	51.550	0.182	0.019	-91.271	110.802	0.850	141	11
		NDWI	-25.713	5.158	-2.650	0.103	-35.822	-15.605	0.000	153	12

https://doi.org/10.5194/egusphere-2026-2639
Preprint. Discussion started: 2 June 2026

Table B1 continued

Method	Class	Treatm.	Effect	SE	Effect Std	SD Treatm.	CI_{Lower}	CI_{Upper}	p	N	Sites
		FireDays	0.000	0.000		0.000	0.000	0.000	0.901	82	6
		HWD	-0.194	0.316	-1.056	5.459	-0.812	0.425	0.540	151	12
		$NDVI_{summer}$	72.663	44.660	1.942	0.027	-14.869	160.194	0.104	82	6
		ROS	-1.699	0.998	-3.383	1.991	-3.656	0.257	0.089	151	12
	Tr	TDD	0.031	0.021	5.378	171.695	-0.010	0.073	0.139	56	2
		FDD	-0.008	0.005	-4.092	520.793	-0.017	0.001	0.100	56	2
		SWE_{max}	6.089	34.976	0.181	0.030	-62.462	74.641	0.862	56	2
		SDO	-0.263	0.257	-1.818	6.903	-0.766	0.240	0.305	56	2
		P_{summer}	0.026	0.006	1.332	51.241	0.015	0.037	0.000	56	2
		SM	-182.920	316.259	-4.462	0.024	-802.777	436.937	0.563	56	2
		NDWI	12.505	2.587	0.984	0.079	7.434	17.576	0.000	54	2
		HWD	0.684	0.544	3.920	5.734	-0.382	1.749	0.209	56	2
		ROS	-4.081	0.491	-3.157	0.773	-5.044	-3.119	0.000	56	2
FD	All	TDD	0.013	0.004	2.381	180.930	0.006	0.020	0.000	1704	97
		FDD	-0.002	0.001	-0.800	491.116	-0.004	0.000	0.132	1704	97
		SWE_{max}	11.966	7.998	0.731	0.061	-3.709	27.642	0.135	1704	97
		SDO	-0.058	0.057	-0.478	8.234	-0.170	0.054	0.311	1704	97
		P_{summer}	0.027	0.008	1.723	63.181	0.011	0.044	0.001	1704	97
		SM	-40.047	23.544	-0.891	0.022	-86.192	6.097	0.089	1594	89
		NDWI	-6.423	2.827	-0.742	0.115	-11.964	-0.883	0.023	2064	119
		FireDays	1.689	1.241	0.106	0.063	-0.744	4.121	0.174	1254	74
		HWD	0.024	0.069	0.187	7.917	-0.112	0.159	0.732	1704	97
		$NDVI_{summer}$	28.859	11.817	1.551	0.054	5.699	52.019	0.015	1201	71
		ROS	-0.684	0.325	-1.496	2.189	-1.320	-0.047	0.035	1704	97
	RT	TDD	0.012	0.011	2.426	208.432	-0.010	0.033	0.284	252	18
		FDD	0.001	0.002	0.523	554.391	-0.004	0.005	0.678	252	18
		SWE_{max}	5.637	12.257	0.563	0.100	-18.387	29.661	0.646	252	18
		SDO	-0.103	0.200	-0.952	9.212	-0.496	0.289	0.605	252	18
		P_{summer}	0.035	0.015	2.390	68.933	0.006	0.063	0.017	252	18
		SM	-144.867	100.106	-2.558	0.018	-341.070	51.337	0.148	219	15

https://doi.org/10.5194/egusphere-2026-2639
Preprint. Discussion started: 2 June 2026

Table B1 continued

Method	Class	Treatm.	Effect	SE	Effect Std	SD Treatm.	CI_{Lower}	CI_{Upper}	p	N	Sites
		NDWI	-17.212	9.252	-2.236	0.130	-35.346	0.922	0.063	297	20
		FireDays	-7.668	5.434	-0.310	0.040	-18.318	2.982	0.158	174	11
		HWD	0.156	0.182	1.546	9.892	-0.201	0.514	0.391	252	18
		$NDVI_{summer}$	56.413	63.260	2.388	0.042	-67.575	180.401	0.373	161	10
		ROS	-1.095	0.823	-3.456	3.157	-2.708	0.519	0.184	252	18
	GT	TDD	0.028	0.007	4.774	167.930	0.014	0.043	0.000	425	21
		FDD	-0.006	0.003	-2.640	441.495	-0.013	0.001	0.083	425	21
		SWE_{max}	2.877	11.616	0.175	0.061	-19.889	25.644	0.804	425	21
		SDO	-0.266	0.100	-1.867	7.012	-0.461	-0.071	0.008	425	21
		P_{summer}	0.012	0.026	0.746	61.936	-0.039	0.063	0.642	425	21
		SM	-67.457	64.653	-1.365	0.020	-194.174	59.260	0.297	408	20
		NDWI	-7.505	4.099	-0.945	0.126	-15.538	0.528	0.067	689	34
		FireDays	0.000	0.000		0.000	0.000	0.000	0.878	329	18
		HWD	-0.001	0.219	-0.006	5.347	-0.431	0.429	0.996	425	21
		$NDVI_{summer}$	25.706	21.046	1.718	0.067	-15.544	66.956	0.222	312	17
		ROS	-0.041	0.411	-0.090	2.214	-0.846	0.764	0.921	425	21
	NT	TDD	0.007	0.005	1.309	181.453	-0.002	0.016	0.111	791	41
		FDD	0.000	0.001	-0.164	484.384	-0.002	0.002	0.721	791	41
		SWE_{max}	25.972	12.073	1.241	0.048	2.310	49.634	0.031	791	41
		SDO	-0.046	0.067	-0.410	8.837	-0.177	0.084	0.485	791	41
		P_{summer}	0.033	0.009	2.083	63.199	0.016	0.050	0.000	791	41
		SM	-22.589	25.279	-0.546	0.024	-72.134	26.956	0.372	741	38
		NDWI	1.389	6.044	0.132	0.095	-10.457	13.235	0.818	843	48
		FireDays	2.394	0.441	0.210	0.088	1.529	3.259	0.000	608	35
		HWD	-0.033	0.071	-0.278	8.447	-0.172	0.106	0.642	791	41
		$NDVI_{summer}$	29.717	11.968	1.550	0.052	6.261	53.174	0.013	585	34
		ROS	-0.555	0.395	-0.953	1.716	-1.329	0.219	0.160	791	41
	GTh	TDD	0.009	0.005	1.454	163.611	-0.002	0.020	0.104	151	12
		FDD	-0.002	0.004	-1.079	476.387	-0.011	0.006	0.595	151	12
		SWE_{max}	46.104	44.897	2.324	0.050	-41.892	134.100	0.304	151	12

https://doi.org/10.5194/egusphere-2026-2639
Preprint. Discussion started: 2 June 2026

Table B1 continued

Method	Class	Treatm.	Effect	SE	Effect Std	SD Treatm.	CI_{Lower}	CI_{Upper}	p	N	Sites
		SDO	0.110	0.274	0.775	7.040	-0.427	0.647	0.688	151	12
		P_{summer}	0.031	0.020	1.581	51.056	-0.009	0.070	0.124	151	12
		SM	-23.318	29.642	-0.533	0.023	-81.415	34.779	0.431	141	11
		NDWI	-6.105	3.901	-0.871	0.143	-13.750	1.541	0.118	153	12
		FireDays	0.000	0.000		0.000	0.000	0.000	0.089	82	6
		HWD	-0.032	0.233	-0.261	8.073	-0.489	0.424	0.889	151	12
		$NDVI_{summer}$	73.400	21.398	2.443	0.033	31.461	115.339	0.001	82	6
		ROS	-1.789	0.852	-4.941	2.762	-3.459	-0.118	0.036	151	12
	Tr	TDD	0.011	0.018	2.308	217.359	-0.024	0.045	0.545	56	2
		FDD	-0.002	0.001	-1.016	634.136	-0.004	0.001	0.253	56	2
		SWE_{max}	-46.342	45.899	-1.683	0.036	-136.302	43.618	0.313	56	2
		SDO	0.119	0.115	1.016	8.568	-0.106	0.344	0.302	56	2
		P_{summer}	0.029	0.003	1.980	68.631	0.023	0.034	0.000	56	2
		SM	-48.313	112.112	-1.191	0.025	-268.048	171.423	0.667	56	2
		NDWI	13.438	0.916	1.297	0.097	11.642	15.234	0.000	54	2
		HWD	0.416	0.256	3.550	8.534	-0.085	0.917	0.104	56	2
		ROS	-3.188	0.716	-3.306	1.037	-4.592	-1.785	0.000	56	2

https://doi.org/10.5194/egusphere-2026-2639
Preprint. Discussion started: 2 June 2026

Table B2. DAG specifications for causal inference of ALT drivers. Confounders satisfy the backdoor criterion (causally affect both treatment and ALT) and form the minimal sufficient adjustment set. Mediators lie on the causal pathway from treatment to ALT and are excluded from adjustment to avoid biasing effect estimates.

Treatment	Confounders (Adjustment Set)	Mediators (Not Adjusted)
TDD	Lat, Elevation, Distance to Coast, Continentality, Slope, Aspect	Soil T, SM, NDVI_{summer}, LAI Summer, NDWI Annual
FDD	Lat, Elevation, Continentality, Slope, Aspect, Wind Direction Winter, Wind Speed Winter	Soil T Winter Mean, Soil T Winter Min
SWE_{max}	P Annual, Lat, Elevation, Wind Direction Winter, Wind Speed Winter, Slope, Aspect, TPI, Landform, Land Cover, LAI Summer, MAAT, FDD	Soil T Winter Mean, Snow Depth Winter, SDO
SDO	Lat, Elevation, MAAT, Aspect, Slope, SWE_{max}	TDD
P_{summer}	Lat, Elevation, Distance To Coast, Continentality, Slope, TPI, Landform	SM, NDWI, NDVI_{summer}, LAI Summer
SM	TPI, Slope, Landform, Soil Texture 0cm, SOC 0cm, P_{summer}	Soil T, NDWI
NDWI	TPI, Slope, Landform, Soil Texture 0 cm	SM, Soil T
FireDays	Land Cover, T Summer Max, HWD, Distance to Coast, Continentality, Lat, TDD	NDVI_{summer}, LAI Summer, Albedo Annual, SM
HWD	Lat, Elevation, Continentality, T Annual Range	Soil T, SM
NDVI_{summer}	Lat, MAAT, P_{summer}, Soil Texture 0cm, SOC 0cm, Land Cover, FireDays	LAI Summer, SM, Albedo Annual
ROS	P Annual, T Winter Mean, Lat, Elevation, Distance to Coast, Continentality	Snow Depth Max, Soil T Winter Mean

Author contributions. A. Ahajjam: Conceptualization, Methodology, Investigation, Writing – original draft, Writing – review & editing, and Visualization. M. Soaper: Conceptualization, Data curation, Investigation and Validation, Writing – original draft, Writing – review & editing. U. Gupta: Methodology, Investigation and Validation, Writing – original draft, Writing – review & editing. A. Wilcox: Investigation, Writing – original draft, and Writing – review & editing. A. Caparó Bellido: Investigation and Validation, and Writing – review & editing. S. Weaver: Investigation and Validation, Writing – review & editing. S. Kidanu: Supervision, Investigation and Validation, Writing – review & editing. D. Nicolsky: Supervision, Investigation and Validation, Writing – review & editing. T. Pasch: Funding acquisition, Supervision, Writing – review & editing, Conceptualization, and Resources.

https://doi.org/10.5194/egusphere-2026-2639
Preprint. Discussion started: 2 June 2026

Competing interests. The authors declare that they have no conflict of interest.

Acknowledgements. DISTRIBUTION A: Approved for Public Release. Distribution is Unlimited. This material is based upon work supported by the Broad Agency Announcement Program and the Cold Regions Research and Engineering Laboratory (ERDC-CRREL) under Contract No. W913E524C0017.

https://doi.org/10.5194/egusphere-2026-2639
Preprint. Discussion started: 2 June 2026

References

Ahajjam, A.: MOREDataset/ALDI: Datasets and Scripts, https://doi.org/10.5281/zenodo.20497762, 2026.

Angrist, J. D. and Pischke, J.-S.: Mostly Harmless Econometrics: An Empiricist's Companion, Princeton University Press, ISBN 978-0-691-12035-5, 2009.

Biskaborn, B. K., Smith, S. L., Noetzli, J., Matthes, H., Vieira, G., Streletskiy, D. A., Schoeneich, P., Romanovsky, V. E., Lewkowicz, A. G., Abramov, A., et al.: Permafrost is warming at a global scale, Nature communications, 10, 264, 2019a.

Biskaborn, B. K., Smith, S. L., Noetzli, J., et al.: Permafrost is warming at a global scale, Nature Communications, 10, 264, https://doi.org/10.1038/s41467-018-08240-4, 2019b.

Brown, J., Hinkel, K. M., and Nelson, F. E.: The Circumpolar Active Layer Monitoring (CALM) program: Research designs and initial results, Polar Geography, 24, 166–258, https://doi.org/10.1080/10889370009377698, 2000.

Cameron, A. C. and Miller, D. L.: A Practitioner's Guide to Cluster-Robust Inference, Journal of Human Resources, 50, 317–372, https://doi.org/10.3368/jhr.50.2.317, 2015.

Carlson, R. E. and Fritsch, F. N.: An algorithm for monotone piecewise bicubic interpolation, SIAM Journal on Numerical Analysis, 26, 230–238, 1989.

Chard, K., Tuecke, S., and Foster, I.: Globus: Recent enhancements and future plans, in: Proceedings of the XSEDE16 Conference on Diversity, Big Data, and Science at Scale, pp. 1–8, 2016.

Gao, B.-C.: NDWI—A normalized difference water index for remote sensing of vegetation liquid water from space, Remote sensing of environment, 58, 257–266, 1996.

Hamed, K. H. and Rao, A. R.: A modified Mann-Kendall trend test for autocorrelated data, Journal of hydrology, 204, 182–196, 1998.

Heginbottom, J., Brown, J., Melnikov, E., and Ferrians Jr, O.: Circumarctic map of permafrost and ground ice conditions, in: Proceedings of the Sixth International Conference on Permafrost, vol. 2, pp. 1132–1136, South China University of Technology Press Wushan Guangzhou, China, 1993.

Heginbottom, J., Brown, J., Ferrians, O., and Melnikov, E.: Circum-Arctic Map of Permafrost and Ground-Ice Conditions, Version 2, https://doi.org/10.7265/SKBG-KF16, 2002.

Hjort, J., Streletskiy, D., Doré, G., Wu, Q., Bjella, K., and Luoto, M.: Impacts of permafrost degradation on infrastructure, Nature Reviews Earth & Environment, 3, 24–38, https://www.nature.com/articles/s43017-021-00247-8, 2022.

Jorgenson, M. T., Shur, Y. L., and Pullman, E. R.: Abrupt Increase in Permafrost Degradation in Arctic Alaska, Geophysical Research Letters, 33, L02 503, https://doi.org/10.1029/2005GL024960, 2006.

Kendall, M. G.: Rank Correlation Methods, Charles Griffin, London, 4th edn., 1975.

Klene, A. E., Nelson, F. E., Shiklomanov, N. I., and Hinkel, K. M.: The n-factor in natural landscapes: variability of air and soil-surface temperatures, Kuparuk River Basin, Alaska, USA, Arctic, Antarctic, and Alpine Research, 33, 140–148, 2001.

Künsch, H. R.: The Jackknife and the Bootstrap for General Stationary Observations, The Annals of Statistics, 17, 1217–1241, https://doi.org/10.1214/aos/1176347265, 1989.

Ling, F. and Zhang, T.: Impact of the timing and duration of seasonal snow cover on the active layer and permafrost in the Alaskan Arctic, Permafrost Periglac. Processes, 14, 141–150, 2003.

Luo, D., Wu, Q., Jin, H., Marchenko, S. S., Lü, L., and Gao, S.: Recent changes in the active layer thickness across the northern hemisphere, Environmental Earth Sciences, 75, 555, 2016.

https://doi.org/10.5194/egusphere-2026-2639
Preprint. Discussion started: 2 June 2026

Mann, H. B.: Nonparametric tests against trend, Econometrica, 13, 245–259, https://doi.org/10.2307/1907187, 1945.

Muñoz Sabater, J., Dutra, E., Agustí-Panareda, A., Albergel, C., Arduini, G., Balsamo, G., Boussetta, S., Choulga, M., Harrigan, S., Hersbach, H., Martens, B., Miralles, D. G., Piles, M., Rodríguez-Fernández, N. J., Zsoter, E., Buontempo, C., and Thépaut, J.-N.: ERA5-Land: a state-of-the-art global reanalysis dataset for land applications, Earth System Science Data, 13, 4349–4383, https://doi.org/10.5194/essd-13-4349-2021, 2021.

Mudelsee, M.: Trend analysis of climate time series: A review of methods, Earth-Science Reviews, 190, 310–322, https://doi.org/10.1016/j.earscirev.2018.12.005, 2019.

Muller, S. W.: ... Permafrost, Or Permanently Frozen Ground: And Related Engineering Problems, Army map service, U. S. Army, google-Books-ID: ctdQAQAAIAAJ, 1945.

Nelson, F. E., Shiklomanov, N. I., and Nyland, K. E.: Cool, CALM, collected: the Circumpolar Active Layer Monitoring program and network, Polar Geography, 44, 155–166, 2021.

Obu, J.: How Much of the Earth's Surface is Underlain by Permafrost?, Journal of Geophysical Research: Earth Surface, 126, e2021JF006 123, https://doi.org/10.1029/2021JF006123, _eprint: https://onlinelibrary.wiley.com/doi/pdf/10.1029/2021JF006123, 2021.

Osterkamp, T.: Characteristics of the recent warming of permafrost in Alaska, Journal of Geophysical Research: Earth Surface, 112, 2007.

O'Neill, H. B., Smith, S. L., Burn, C. R., Duchesne, C., and Zhang, Y.: Widespread Permafrost Degradation and Thaw Subsidence in Northwest Canada, Journal of Geophysical Research: Earth Surface, 128, e2023JF007 262, https://doi.org/10.1029/2023JF007262, 2023.

Pearl, J.: [Bayesian analysis in expert systems]: Comment: Graphical models, causality and intervention, Statistical Science, 8, 266–269, 1993.

Peng, X., Zhang, T., Frauenfeld, O. W., Wang, K., Luo, D., Cao, B., Su, H., Jin, H., and Wu, Q.: Spatiotemporal Changes in Active Layer Thickness under Contemporary and Projected Climate in the Northern Hemisphere, Journal of Climate, 31, 251 – 266, https://doi.org/10.1175/JCLI-D-16-0721.1, 2018.

Romanovsky, V. E. and Osterkamp, T. E.: Thawing of the Active Layer on the Coastal Plain of the Alaskan Arctic, Permafrost and Periglacial Processes, 8, 1–22, https://doi.org/10.1002/(SICI)1099-1530(199701)8:1<1::AID-PPP243>3.0.CO;2-U, 1997.

Romanovsky, V. E., Drozdov, D., Oberman, N. G., Malkova, G., Kholodov, A. L., Marchenko, S., Moskalenko, N. G., Sergeev, D., Ukraintseva, N., Abramov, A., et al.: Thermal state of permafrost in Russia, Permafrost and Periglacial Processes, 21, 136–155, 2010.

Sen, P. K.: Estimates of the regression coefficient based on Kendall's tau, Journal of the American Statistical Association, 63, 1379–1389, https://doi.org/10.1080/01621459.1968.10480934, 1968.

Shiklomanov, N. I., Streletskiy, D. A., Nelson, F. E., Hollister, R. D., Romanovsky, V. E., Tweedie, C. E., Bockheim, J. G., and Brown, J.: Decadal variations of active-layer thickness in moisture-controlled landscapes, Barrow, Alaska, Journal of Geophysical Research: Biogeosciences, 115, 2010.

Shiklomanov, N. I., Streletskiy, D. A., and Nelson, F. E.: Northern hemisphere component of the global circumpolar active layer monitoring (CALM) program, in: Proc. 10th Int. Conf. on Permafrost, vol. 1, pp. 377–382, 2012a.

Shiklomanov, N. I., Streletskiy, D. A., Nelson, F. E., et al.: Decadal variations of active-layer thickness in moisture-controlled landscapes, Barrow, Alaska, Journal of Geophysical Research: Biogeosciences, 117, G00N05, https://doi.org/10.1029/2011JG001748, 2012b.

Smith, S., Romanovsky, V., Lewkowicz, A., Burn, C., Allard, M., Clow, G., Yoshikawa, K., and Throop, J.: Thermal state of permafrost in North America: a contribution to the international polar year, Permafrost and Periglacial Processes, 21, 117–135, 2010.

Smith, S. L., O'Neill, H. B., Isaksen, K., Noetzli, J., and Romanovsky, V. E.: The changing thermal state of permafrost, Nature Reviews Earth & Environment, 3, 10–23, 2022.

https://doi.org/10.5194/egusphere-2026-2639
Preprint. Discussion started: 2 June 2026

Streletskiy, D. A., Sherstiukov, A. B., Frauenfeld, O. W., and Nelson, F. E.: Changes in the 1963–2013 shallow ground thermal regime in Russian permafrost regions, Environmental Research Letters, 10, 125 005, 2015.

Streletskiy, D. A., Biskaborn, B. K., Smith, S. L., Noetzli, J., Vieira, G., and Schoeneich, P.: GTN-P Strategy and Implementation Plan 2016–2020, Technical report, Global Terrestrial Network for Permafrost, 2017.

Streletskiy, D. A., Clemens, S., Lanckman, J.-P., and Shiklomanov, N. I.: The costs of Arctic infrastructure damages due to permafrost degradation, Environmental Research Letters, 18, 015 006, https://iopscience.iop.org/article/10.1088/1748-9326/acab18/meta, publisher: IOP Publishing, 2023.

SUSE Rancher: What is Rancher?, https://ranchermanager.docs.rancher.com/, accessed: March 26, 2026, 2023.

Wilcox, A., Moradi, M., Miller, S., Parker, S., Nesbitt, I., Bergstrom, A., Kaabouch, N., and Pasch, T.: The arctic knowledge-based system: Science gateway integration for petascale arctic data processing and geospatial feature prediction, Applied Computing and Geosciences, p. 100322, 2026.

Zhang, T.: Spatial and temporal variability in active layer thickness over the Russian Arctic drainage basin, J. Geophys. Res., 110, D16 101, 2005.

Zhang, T., Osterkamp, T. E., and Stamnes, K.: Influence of the depth hoar layer of the seasonal snow cover on the ground thermal regime, Water Resour. Res., 32, 2075–2086, 1996.

Zonca, A. and Sinkovits, R. S.: Deploying Jupyter Notebooks at scale on XSEDE resources for Science Gateways and workshops, in: Proceedings of the Practice and Experience on Advanced Research Computing: Seamless Creativity, PEARC '18, Association for Computing Machinery, New York, NY, USA, ISBN 9781450364461, https://doi.org/10.1145/3219104.3219122, 2018.